Effect of Specific Surface Area of In-Process Calcined Powder on Electrical and Magnetic Properties of Finished Mn-Zn ferrites

A thesis Submitted

In the partial fulfillment of the

Requirement of the Degree of

Master of Technology

IN

Materials Science and Engineering

Submitted by

SANDEEP KUMAR SINGH

(60702018)

Under the guidance of

Prof. O.P. Pandey and Mr. Sameer Yadav

School of Physics and Materials Science

THAPAR UNIVERSITY

PATIALA, PUNJAB- 147004

JUNE-2009

Dedicated To My Parents

CERTIFICATE

This is to certify that the thesis entitled, "**Effect of Specific Surface Area of In-Process Calcined Powder on Electrical and Magnetic Properties of Finished Mn-Zn ferrites"**, submitted by **Mr. Sandeep Kumar Singh** in the partial fulfillment of the requirement for the award of the degree of M. Tech in **Materials Science and Engineering** from the **School of Physics and Materials Science, Thapar University, Patiala**, is a record of candidate's own work carried out by him under our supervision and guidance. The matter embodied in this thesis has not been submitted in part or full to any other university or institute for the award of any degree.

The thesis work has been carried out from 01.01.2009 to 30.06.2009.

Supervisors

(Dr. O.P Pandey)
Prof. & Head
School Of Physics and Materials Science
Thapar University, Patiala
Punjab -147004

(Mr. Sameer Yadav)
Manager (R&D)
Cosmo Ferrites Limited
Jabli, Solan
Himachal Pradesh -173209

Countersigned by:

Dr. O.P Pandey
Prof. & Head
School Of Physics and Materials Science
Thapar University, Patiala

Dr .R. K. Sharma 24/7/09
Dean, Academic Affairs
Thapar University, Patiala

ACKNOWLEDGEMENT

I visualize a rare movement of pride and pleasure to extend my sincere and heedful gratitude to my Guides **Dr. O.P Pandey, Professor and Head, School of Physics and Materials Science, Thapar university** and **Mr. Sameer Yadav, Manager, R&D, Cosmo Ferrites Limited** for their keen interest and valuable guidance, strong motivation and constant encouragement during the course of the work. I thank them from the bottom of my heart for providing me exposure to the latest Research and Developments in the field of Ferrite Materials. I, infact find paucity of words to express his sound knowledge of the subject and keen interest in it and his potential during the course of the work.

I am grateful to **Mr. Arun Yadav (G.M.), Mr. K. Sriram, Mr. Sanjeev Katoch, Cosmo Ferrites Limited**, for his encouragement, which will forever remain a driving force for me.

My greatest thanks are to **Dr. K.K.Raina**, **Deputy Director, Thapar University** and **Dr. N. K. Verma, Dean Student Affairs, Thapar University** for their full motivation and appreciation to my work. They provide me moral support as well as necessary help during my experimental work.

I am highly greatful to **Dr. Kulvir Singh**, **Asst. Prof. School Of Physics And Material Science, Thapar University, Patiala (Punjab)** for their kind help and valuable suggestions and special attention throughout my work. It is due to his moral encouragement, love and providing me fountain of inspiration, all sorts of assistance from time to time into up-bringing me up to this stage.

I wish to express my warm and sincere thanks to **Mr. Vishal Chaudhary, Ms Kamal Waraich, Mr. Pursottam Singh, Inder Mani** and all members of School of Physics and Material Science.

I wish to express thanks to **Mr. Ashish Gautam, Mrs. Lata Katoch, Mr. Arun Kumar, Mr. Charanjeet, Mr. Hemraj** and all members of R&D, Cosmo Ferrites Limited, who has given their support during my experimental work.

I wish to express my warm and sincere thanks to all my friends who devoted their valuable time and helped me in all possible ways towards successful completion of

this work. Thanks are very small words for my dearest friends **Mr. Karuna Sagar Chaturvedi, Mr. Arun Kumar Singh, Mr. Neetesh Kumar and Ms Indu Bajpai** whose ideas and concepts have had a remarkable influence on my understanding in the field of Material Science and Engineering.

I would like to thank my parents and my whole family whose honest support and obstinate love give me energy to complete this work successfully and gave me untiring help during my difficult moments.

Date: 14-07-2009

Place: Patiala

Sandeep Kumar Singh

(Roll.No.-60702018)

ii

ABSTRACT

The technology of ferrites or magnetic ceramics has assumed a new importance during the last several decades and especially in the last few years. In addition to the advent of new developments such as radars, satellite communications, memory and computer applications, there has been a corresponding growth in consumer electronics markets in radio, television, power inverters etc.

In this thesis work, Mn-Zn ferrite core of the basic composition of 51.96 mole% ferric oxide , 37.88 mole% manganese oxide and remaining 10.16 mole% zinc Oxide and other composition is 50.78 mole% ferric oxide, 27.18 mole% manganese oxide and remaining 22.04 mole% zinc Oxide have been synthesized by conventional route. These ferrites have been investigated for their specific surface area (SSA), electrical and magnetic properties such as initial permeability, resistance and power loss.

The specific surface area plays an important role for the electrical and magnetic properties of Mn-Zn Ferrite. This has great influence on green and sintered strength. According for the required properties can be achieved with optimum ball milling time and attritor time. Specific surface area increases and particle size decreases with increases of milling time of ball milling and attritor.

For low power loss materials, specific surface area affects electrical and magnetic property as at 5159 cm^2/gm SSA exhibits low power loss ($69kw/m^3$) and low resistance while at 5468 cm^2/gm power loss increases ($74kw/m^3$) and resistance also increase. For high permeability (μ_i) material, at 10 KHz frequency and SSA 5359 cm^2/gm initial permeability exhibits higher (8960nH) and while at $5562cm^2/gm$ initial permeability decreases (7906 nH). At 100 kHz frequency and SSA 5359 cm^2/gm initial permeability exhibits higher (7739nH), while at $5562cm^2/gm$ initial permeability decrease (6917nH).

CONTENTS

LIST OF FIGURES

Chapter 1 — Page Number

Chapter 2

Chapter-3

Chapter-4

LIST OF TABLES

CHAPTER 1
INTRODUCTION

1.1 History

Ferrites are dark grey or black ceramic materials. They are very hard, brittle and chemically inert. Most modern magnetically soft ferrites have a cubic (spinel) structure. Earlier Iron and its alloys were used as magnetic materials for the applications in the electrical industry. However, with the discovery of higher frequencies, the customary techniques to reducing eddy current losses, using lamination or iron powder cores, were no longer efficient or cost effective. This realization stimulated a renewed interest in "magnetic insulators" as first reported by S. Hilpert in Germany in 1909. It was readily understood that if the high electrical resistivity of oxides could be combined with desired magnetic characteristics, a magnetic material would result that was particularly well suited for high frequency operation. These materials are called ferrites which have general formula MFe_3O_4 where M is the divalent ion like Zn^{++}, Mn^{++}.

These ferrites are homogeneous ceramic materials composed of various oxides with iron oxide as their main constituent and fall in the category of soft and hard ferrites. Based upon the chemical composition, soft ferrites can be divided into two major categories, manganese-zinc ferrites and nickel-zinc ferrites. In each of these categories many different Mn-Zn and Ni-Zn material grades are being manufactured by varying the chemical composition or by different manufacturing techniques. These compounds exhibit good magnetic properties below a certain temperature called the Curie temperature. They can easily be magnetized and have a rather high intrinsic resistivity. The two families of Mn-Zn and Ni-Zn ferrite materials complement each other and allow the use of soft ferrites from audio frequencies to several hundred mega-hertz. The first practical application of soft ferrite was in inductors which were used in LC filters in frequency division multiplex equipment. The combination of high resistivity and good magnetic properties made these ferrites an excellent core material for these filters operating over the 50-450 kHz frequency range. The large scale introduction of TV in the 1950's was a major opportunity for the fledgling ferrite industry. In TV sets, ferrite cores were the material of choice for the high

voltage transformer and the picture tube deflection system. For four decades ferrite components have been used in an ever widening range of applications and in steadily increasing quantities, a few are mentioned in Table 1.1 below.

Table 1.1 A applications of soft ferrites

Magnetic device	**Applications**
Power transformers and Chokes	High frequency power supplies
Inductors and tuned transformers	Frequency selective circuits
Pulse and wide band transformers	Matching devices
Magnetic deflection structures	TV sets and monitors
Recording heads	Memory storage devices
Rotating transformers	VCR's
Transducers	Vending machines and ultrasonic cleaners

Table 1.2 Merits and demerits of ferrites over other magnetic materials.

Advantages	**Disadvantages**
High resistivity	Low saturation flux density
Wide range of operating frequencies	Poor thermal conductivity
Low loss combined with high permeability	Low tensile strength
Time and temperature stability	Brittle material
Large material selection	
Versatility of core shapes and low cost	

These cubic ferrites are especially useful due to two key characteristics [1]

- ❖ High magnetic permeability, which concentrates and enhances the magnetic field.
- ❖ High electrical resistivity, which ensures total penetration of the electromagnetic (EM) field.

Furthermore, the dominance of ferrites rests upon a remarkable flexibility in providing tailor-made solutions, ease of fabrication, and price and performance considerations. Hence ferrites are widely manufactured into circuit elements like inductors and cores, reading-writing heads and information storage media.

Amongst the soft ferrites, Manganese Zinc Ferrites are most common, and are used in many more applications than their counterparts, such as nickel-zinc ferrites. Within the Mn-Zn category, large varieties of materials are possible and the material selection is mainly a function of the application that needs to be accommodated. The application dictates the desirable material characteristics which in turn determine the chemical composition of the ferrite material. Manganese zinc ferrites are primarily used for frequencies less than 2 MHz Figure-1.1 shows the composition diagram for Mn-Zn ferrites in mole% for Ferric oxide, Manganese oxide and Zinc oxide.[2]

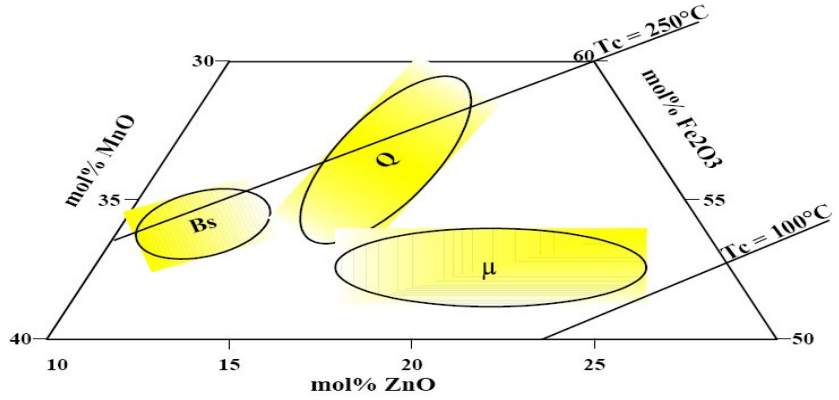

Figure 1.1 Composition Diagram for Mn-Zn ferrites.

It identifies the composition which gives optimum performance for saturation flux density (B_s), low losses (Q) and high initial permeability (μ_i). It also identifies the Curie temperature (T_C) lines for 100 and 250°C. From this composition chart, it is clear that not one composition, of Mn ferrite, can fulfill all design objectives.

Bs- Compositions of higher saturation

Q- Composition of higher Q

μ – Composition of higher initial permeability

Nickel-Zinc ferrites are characterized by their high material resistivity which is several orders of magnitude higher than Mn-Zn ferrites. Because of its high resistivity Ni-Zn ferrite is the material of choice for operating from l-2 MHz. to several hundred MHz. To cover such a wide frequency range and different applications, a large number of Nickel-Zinc materials have been developed over the years. Use of Nickel-Zinc ferrites is limited due to their increasing cost. It should be noted that certain nickel chemistries are stress sensitive and can be adversely changed by some types of stress; this may be a mechanical shock or any grinding operations. Strong magnetic fields from holding devices and fixtures or magnetic chucks used in machining operations may also provide this stress. These resulting changes can include variation in permeability and core loss (lowering of Q). These changes cannot be reversed by degaussing or other electric/magnetic processes.

Manganese -Zinc ferrite has the highest permeability and saturation induction of the ferrite class of materials and has the advantage of various stoichiometries with nearly zero magneto-crystalline anisotropy and magneto-restriction, important for stress insensitivity and low noise.

At high frequencies, these soft ferrites have substantial advantages over conventional metallic materials, either in lamination or in powder forming technology. Ferrites offer additional mechanical features as well. Ferrites can be shaped in a variety of different core geometries optimized for specific applications. For example, cores can be designed for ease of assembly, or made self-shielding where required. Power applications require the transfer of power through the magnetic device, which requires operation of ferrite at high flux density and elevated temperature in the core. Magnetic components of ferrites are used for various applications throughout the industry. The magnetic function of these components in power applications is normally a transformer or inductor.

Main application areas and function for power ferrites are listed as in:

- Automotive Electronics
- Consumer Electronics

- Electronic Data Processing
- Electric Tools
- Household Appliances
- Measurement and control
- Power Conversion
- Telecommunication

With the advent of switched-mode power supplies, the demand for ferrites in power applications has increased significantly. The trend in high frequency power supplies is to go to higher frequencies, which results in size reduction of the magnetic components. This challenge can only be met with soft ferrites.

Desirable ferrite material characteristics for power applications are:

- High saturation flux Density at elevated temperatures (Operating Temperature).
- Low loss at operating frequency, at high flux density and elevated temperature.
- Minimum losses in the operating temperature range.
- High resistivity to minimize the induced eddy currents.

1.2 Crystal Structures of Ferrites

The crystal structure of ferrites can be regarded as an interlocking networking of positively charged metal ions (Fe^{3+} , M^{2+}) and negatively charged divalent oxygen ions (O^{2-}).The arrangement of the ions or the crystal structure of the ferrite plays an important role in determining the magnetic interactions. [3]

1.3 Classes of Crystal Structures in Ferrites

In ferrites, the crystal structure preferred is determined on the basis of size and charge of the metal ions that balance the charge of oxygen ions and the relative amounts of these ions. There are three crystal structures mostly available in case of ferrites. These are:

- Spinal Structure
- Garnet structure
- Hexa-ferrite structure

1.3.1 Spinal structure

The spinal is by far the most widely used ferrites. The spinal structure is derived from the mineral spinal ($MgAl_2O_4$ or $MgO.Al_2O_3$) whose structure was elucidated by Bragg. Analogous to the mineral spinal the magnetic spinal have general formula $MO.Fe_2O_3$, where M is divalent metal ion. The trivalent aluminium is usually replaced by Fe^{+++} or Fe^{+++} in combination with any other trivalent ion. Although the great majority of ferrites contain iron oxide as name implies, but there are some "ferrites" based on Cr, Mn and other elements. Although Mn, Cr is not ferromagnetic elements, in combination with other elements such as oxygen and other metal ions, they can behave as magnetic ions.

1.3.1.1Ion Charge Balance and Crystal structure

The spinal lattice is composed of a close packed oxygen arrangement in which 32 oxygen ions form a unit cell which is the smallest repeating unit in crystal network. Between the layers of oxygen ions, there are the interstices that may accommodate the metal ions. Not all the interstices are same; some which would be called **A** sites are surrounded with four nearest neighbouring oxygen ions and are called tetrahedral sites. The other of sites (B sites) is coordinated by six neighbouring oxygen ions whose centre connecting lines describe an octahedron. The **B** sites are called octahedral sites. In the unit cell of 32 oxygen ions there are 64 tetrahedral sites and 32 octahedral sites. If all the sites are filled with metal ions, of either +2 or +3 valence, the positive charge would be much greater than the negative charge and so the structure will be much greater than negative charge. Due to which the structure will be electrically neutral. It turns out that of the 64 tetrahedral sites, only 8 are occupied and out of the 32 octahedral sites, only 8 are occupied. If , as in the mineral spinal the tetrahedral are occupied by divalent ions and the octahedral sites are occupied by the trivalent ions, the total positive charge will be $8\times(+2) = +16$ plus the $16 \times (+3) = +48$, or a total of +64 which is needed to balance the $32\times(-2) = -64$ for the oxygen ions. Then there would be eight formula units of $MO.Fe_2O_4$.

1.3.1.2 Site Preference of the Ions

The preference of the individual ions for two types of lattice sites is determined by:

1. The ionic radii of the specific ions
2. The size of interstices

3. Temperature

4. The orbital preference for specific coordination

Table 1.3: Metal ions involved in Spinal ferrites

Metal Ions	Ionic Radius (Angstrom units. A^0)
Mg^{++}	0.78
Mn^{++}	0.91
Mn^{+++}	0.71
Fe^{++}	0.83
Fe^{+++}	0.67
Co^{++}	0.82
Ni^{++}	0.78
Cu^{++}	0.70
Zn^{++}	0.82
Cd^{++}	1.03
Al^{+++}	0.57
Cr^{+++}	0.64

The divalent ions are generally larger than the trivalent, octahedral sites are also larger than tetrahedral, therefore it would be reasonable that trivalent ions go into tetrahedral sites and divalent goes to the octahedral sites. Two exceptions are found in Zn^{++} and Cd^{++} which prefer tetrahedral sites because electronic configuration is favourable for tetrahedral bonding to oxygen ions.

1.3.1.3 Normal Spinals

In a unit cell of spinal lattice, eight tetrahedral and sixteen octahedral sites are occupied by metal ions. In case of mineral spinals the divalent ion (Mg) occupy the **A** site and trivalent ion (Al) occupy the **B** sites, this is known as normal spinal.

1.3.1.4 Inverse Spinals

Barth and Posnak (1915) found many cases in which the trivalent ions preferred the **A** sites and filled these first. Spinals showing this type of structure are known as inverse spinals.

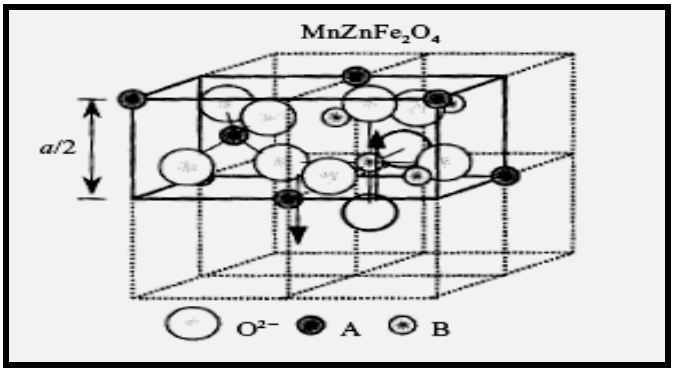

Figure 1.2 Structure of Mn-Zn Ferrite

1.3.2. Hexagonal Ferrites

This class of magnetic oxide is called megnetoplumbite structure from the mineral of the same name. Whereas the symmetry of the spinal crystal structure is cubic, that for the megnetoplumbite structure is hexagonal. Thus, it has a major preferred axis called **C** axis. The preferred direction is used to good advantage for permanent magnetic material.

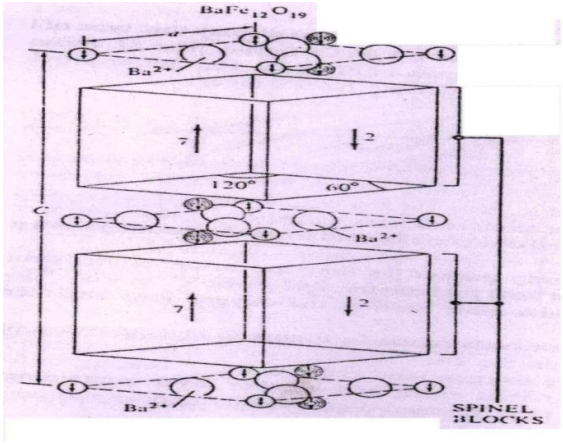

Figure 1.3 Crystal Structure of Hexagonal Mn-Zn Ferrite

The megnetoplumbite unit cell contains a total of ten layers, two of which contain M^{++} ion: four layers of oxygen ions each: followed by a layer of three oxygen ions and one M^{++} ion; again followed by four oxygen layers of four ions each: and another layer containing the three oxygen ions and one M^{++} ion but situated diametrically opposite to the M^{++} ion in the previous layer containing M^{++}.

The Fe^{+++} ions are located in the interstices of these ten layers. There are octahedral and tetrahedral sites, as well as one more type not found in the spinal structure in

which the metal ion is surrounded by five oxygen ions forming a trigonal bi pyramidal in the same layer of the M^{++} ion.

The megnetoplumbite formula is $MFe_{12}O_{19}$, where M can be Ba, Sr, or Pb. There are two formula units per unit cell. Per formula unit, the moments of the 12 Fe^{+++} ions are arranged with the spins of 12 in the up direction and 8 in the down direction, giving a predicted net moment of 4 Fe^{+++} ions per formula unit time 5 per ions, or a total of 20 per formula unit.

1.3.3. Magnetic rare earth garnets

Magnetic garnets crystallize in the dodecahedral or 12-sided structure related to the mineral garnet. The general formula is $3M_2O_35Fe_2O_3$ or $M_3Fe_5O_{12}$. Note that in this case all the metal ions are trivalent in contrast to the other two classes.In the important magnetic garnet, M is usually yttrium (Y) or one of the rare earth ions. Even though

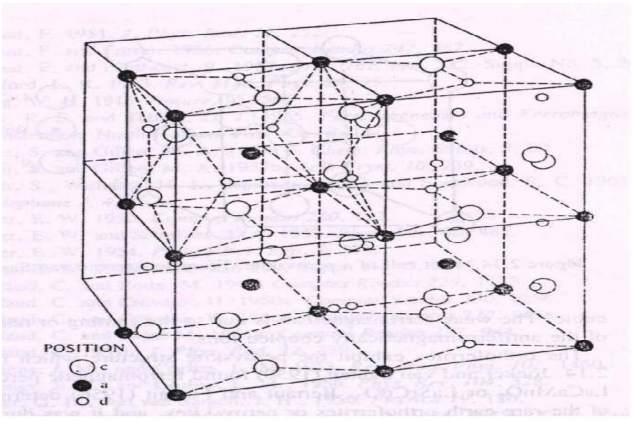

Figure 1.4 Crystal Structure of Magnetic rare earth garnet

yttrium is not a rare earth ion, it behaves as one and therefore is included in the designation rare earth garnets. The ions La^{+++}, Ca^{+++}, Pr^{+++}, and Nd^{+++} are too large to form simple garnets but may form solid solutions with other rare earth garnets.

There are three different types of sites for garnets (a) tetrahedral (b) octahedral; and (c) dodecahedral sites. The unsubstituted garnets that have only trivalent ions are very stoichiometric so that they involve fewer preparation problems compared to the spinels.

The rare earth ions are large, and so they occupy the large dodecahedral sites. There are 16 octahedral, 24 tetrahedral, and 24 dodecahedral sites in a unit cell containing

eight formula units. One formula unit, $3M_2O_35Fe_2O_3$, is distributed as $3M_2O_3$ – dodecahedral (c), $3Fe_2O_3$ –tetrahedral (a), $2Fe_2O_3$-octahedral (d).

1.4 The Magnetization in Domains and Bulk Materials

1.4.1 The nature of domains

In a ferromagnetic domain, there is parallel alignment of the atomic moments. In a ferrite domain, the net moments of the anti-ferrimagnetic interactions are spontaneously oriented parallel to each other (even without an applied magnetic field). Each domain becomes a magnet composed of smaller magnets (ferromagnetic moments). Domains contain about 10^{12} to 10^{15} atoms and their dimensions are on the order of microns ($l0^{-4}$ cm.). Domains are formed to reduce the magnetostatic energy which is the magnetic potential energy contained in the field lines. Figure 1.5 shows the lines of flux in a particle with a single domain.

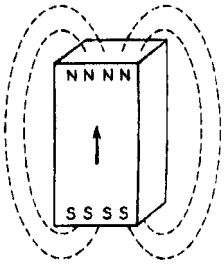

Figure 1.5 Lines of force in a particle of a single domain

The arrows indicate the direction of the magnetization and consequently the direction of spin alignment in the domain. We can substantially reduce the length of the flux path through the unfavourable air space by spitting that domain into two or more smaller domains (Figure 1.6). In Figure 1.6, the moments in adjacent domains called closure domains. When a large domain is split into *n* domains. The energy of the new structure is about *l/n th* of the single domain structure.

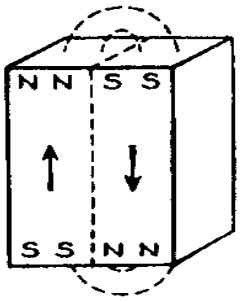

Figure 1.6 Reduction of magnetostatic energy by the formation of domains

The size and shape of a domain may be determined by the minimization of several types of energies. They are;

- Magnetostatic energy
- Magnetocrystalline anisotropy energy
- Magnetostrictive energy
- Domain wall energy

In addition, certain microstructural imperfections such as voids, non-magnetic, inclusions and grain boundaries may also affect the local variations in domain structure.

1.4.2 Magnetostatic Energy

The magnetostatic energy is the work needed to put magnetic poles in special geometric configurations. It is also the energy of demagnetization. It can be calculated for simple geometric shapes. For an infinite sheet magnetized at right angles to the surface the equation (Bozorth 1951) for the magnetostatic energy per cm^3 is;

$$\mathbf{E_p = 2\,\pi M_s^2}$$

Neel (1944) and Kittel (1946) have calculated the magnetostatic energy of flat strips of thickness, d, magnetized to intensity, M, alternately across the thickness of the planes. The equation is;

$$\mathbf{E_p = 0.85\,dM^2}$$

The calculations for other shapes come out with the general formula;

$$\mathbf{E_p = (Constant)\ x\ dM_s^2}$$

Therefore the magnetostatic energy is decreased as the width of the domain decreases.This mathematically confirms the assumption that the splitting of domains into smaller widths decreases the energy from the magnetostatic view

1.4.3 Magnetocrystalline Anisotropy Energy

Most matter is crystalline in nature; that is, it is composed of repeating units of definite symmetry. In most magnetic materials to varying degree, the domain magnetization tends to align itself along one of the main crystal directions. This direction is called the easy direction of magnetization. The difference in energy of a

state where the magnetization is aligned along an easy direction and one where it is aligned along a hard direction is called the magnetocrystalline anisotropy energy.
Magnetocrystalline anisotropy is due to the fact that there is not complete quenching of the orbital angular momentum as we postulated originally. With a small orbital moment that is mechanically tied to the lattice, the spin system can couple to it and therefore indirectly affect the lattice or the dimensions of the material.

1.4.4 Magnetostrictive Energy

When a magnetic material is magnetized, a small change in the dimensions occurs. The relative change is on the order of several parts per million and is called magnetostriction.

The converse is also true. That is, when a magnetic material is stressed, the direction of magnetization will be aligned parallel to the direction of stress in some materials and at right angles to it in others. The energy of magnetostriction depends on the amount of stress and on a constant characteristic of the material called the magnetostriction constant.

$$\mathbf{E = 3/2\ \lambda\sigma}$$

Where; $\boldsymbol{\lambda}$ = magnetostriction constant and $\boldsymbol{\sigma}$ = Applied stress

1.4.5 Domain Wall Energy

Bloch in 1932 presents the idea of magnetic domains, with domain walls (sometimes called Bloch walls) or boundaries separating them. In the domain structure of bulk materials, the domain wall or boundary is that region where the magnetization direction in one domain is gradually changed to the direction of the neighbouring domain. The thickness of the domain wall which is proportional to the number of atomic layers through which the magnetization is to change from the initial direction to the final direction, the exchange energy stored in the transition layer due to the spin interaction is;

$$\mathbf{E_e = kT_c/a}$$

Where $\mathbf{kT_c}$ = thermal energy at the Curie point and a = Distance between atoms
Therefore the exchange energy is reduced by an increase in the width of the wall or with the number of atomic layers in that wall. However, in the presence of an

anisotropy energy or preferred direction, rotation of the magnetization from an easy direction increases the energy so the wall energy due to the anisotropy is:

$$E_k = k\,\delta$$

In this case, the energy is increased as the domain width or number of atomic layers is increased. The two effects oppose each other and the minimum energy of the wall per unit area of wall occurs according to the following equation;

$$E_w = 2\,(K_a T_c/a)^{1/2}$$

Where, K_a = Anisotropy constant

If magnetostriction is a consideration, the equation is modified to;

$$Ew = 2\,(kT/a)^{1/2}\,(K_a + 3\,\lambda_s\sigma/2)^{1/2}$$

Where λs= magnetostriction constant

Typical values of domain wall energies are on the order of **1-2 ergs/cm^2**. The domain wall thickness for the condition of minimum energy is given by the equation;

$$\delta = (\text{constant})\ x\ a\,(E/K)^{1/2}$$

Typical calculated values of **δ** are about 10^3 A^0 or about 10^{-5} cm. With some soft magnetic materials the value may be about 10^{-6} cm while in some hard materials, the value may be on the order of $l0^{-4}$ cm. or about one micron. The whole array of domains will be arranged in such a way as to minimize the total energy of the system composed mainly of the above four energies.

1.4.6 Proof of existence of domains

The earliest experimental indication that domains existed was presented by Barkhausen (1919) who was able to pick up small voltages due to the discontinuous changes in the magnetizations in these regions. Barkhausen amplified these voltages many times and made them audible on a loudspeaker. Bitter (1931) was first able to visualize domains by spreading over the sample, a suspension of colloidal magnetite. The colloidal particles will be concentrated at the domain boundaries since large field gradients exist there. These arrangements are called Bitter patterns. Figure 1.7a exhibits domain walls using this method. This technique is limited to the static state since the powder prohibits true dynamic observations as well as temperature

restrictions. Since light is an electromagnetic wave, it might be expected to interact with magnetic fields and moments Many so-called magneto-optic effects have been observed. Through this interaction

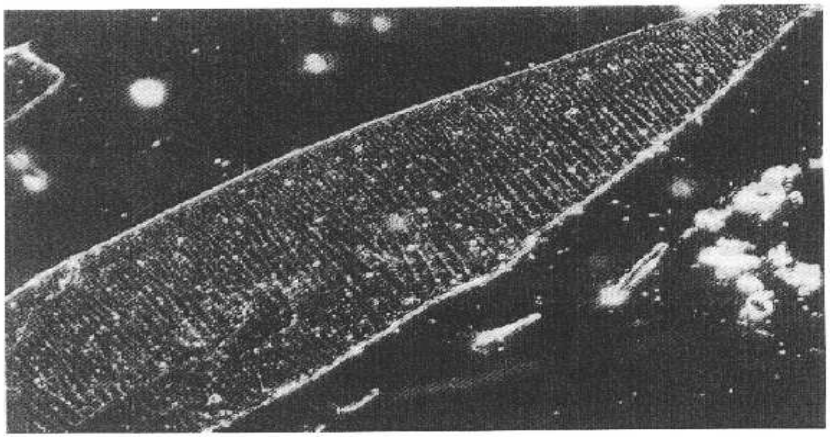

Figure 1.7a Visualization of magnetic domains by means of the Bitter magnetic particle technique. The white stripes are the domain walls.

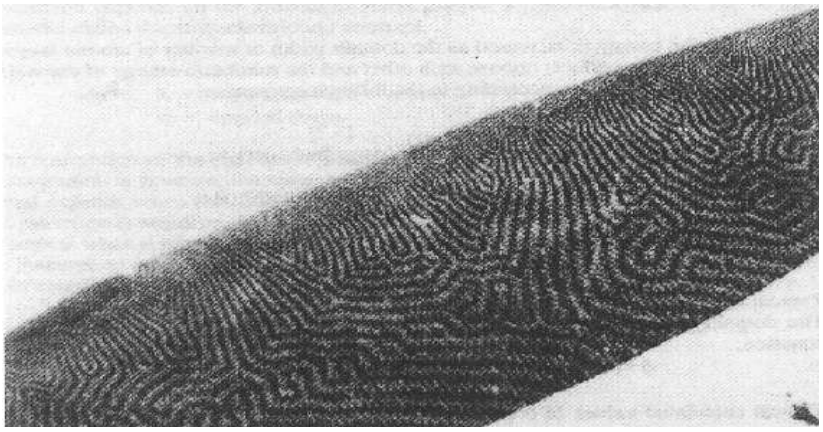

Figure1.7b Visualization of domains by Faraday rotation with polarized light

Domains have been made visible microscopically by both reflected and transmitted light. One technique employs a polarized light which has its plane of polarization rotated differently by domains with different magnetization direction. When the rotated light beam is sent through a polarizing medium called the analyzer, the domains will show up because of the contrast in light intensities of the neighbouring domains. With reflected light, this phenomenon is known as the Kerr effect. With transmitted light, it is called Faraday rotation. Domain patterns in many magnetic materials have been photographed using this technique. Figure 1.7b is an example of

the Faraday technique. Kaczmarek (1992) used the transverse and longitudinal Kerr Effects to observe do-mains in soft polycrystalline ferrites. Using a laser and fibre optics, he examined hysteresis effects that are in good relationship with bulk measurements Domain patterns have also been viewed by TEM (Transmission Electron Microscopy). Vander Zaag (1992) studied domain structures in Mn-Zn ferrites using this technique. He found that at a grain size up to 4 microns, the grains were mono-domain while above this size, they were polydomain.

1.4.7 The dynamic behaviour of domains

Two general mechanisms are involved in changing the magnetization in a domain and, therefore, changing the magnetization in a sample. The first mechanism acts by rotating the magnetization towards the direction of the field. Since this may involve rotating the magnetization from an axis of easy magnetization in a crystal to one of more difficult magnetization, a certain amount of anisotropy energy is required. The rotations can be small as indicated in Figure 1.8 or they can be almost the equivalent

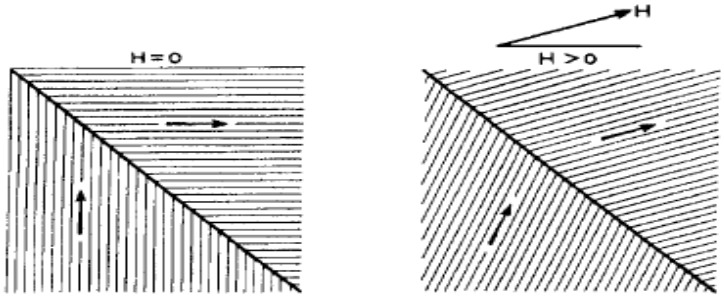

Figure 1.8 Change of domain magnetization by domain wall movement

of a complete 180°reversal or flip if the crystal structure is uniaxial and if the magnetizing field is opposite to the original magnetization direction of the domain. The other mechanism for changing the domain magnetization is one in which the direction of magnetization remains the same, but the volumes occupied by the different domains may change. In this process, the domains whose magnetizations are in a direction closest to the field direction grow larger while those that are more unfavourably oriented shrink in size. This process is called domain wall motion. The mechanism for domain wall motion starts in the domain wall.

Present in the wall is a force (greatest with the moments in the walls that are at an angle of 90° to the applied field) that will tend to rotate those moments in line with

the field. As a result, the center of the domain wall will move towards the domain opposed to the field. Thus, the area of the domain with favourable orientation will grow at the expense of its neighbour.

1.4.8 Bulk behaviour magnetization

We have proceeded through the hierarchy of magnetic structures from the electron through the domain. Although domains are not physical entities such as atoms or crystal lattices and can only visualize by special means, for the purpose of magnetic structure they are important in explaining the process of magnetization. We now can discuss why a material that has strongly oriented moments in a domain often has no

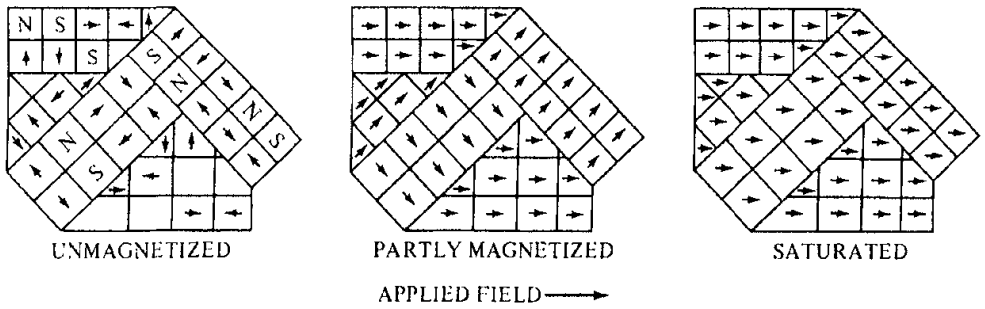

Figure 1.9 Stages in Magnetization of a sample containing several crystals

resultant bulk material magnetization. We can also examine why this apparently "nonmagnetic" material can be transformed into a strongly magnetic body by domain dynamics discussed above. The answer, of course, resides in the fact that, if the material has been demagnetized, the domains point in all random directions so that there is complete cancellation and the resultant magnetization is zero. The possible steps to complete orientation of the domains or magnetization of the material are also shown in Figure 1.9.

1.4.9 The Magnetization Curve

We are now ready to look at the bulk magnetic properties of a material. Thus far, the magnetic moment or the magnetization has been given in either atomic units (or Bohr magnetons) or in physical units based on action of magnets. How can we re-late these to actual material properties? The Bohr magnetons were based on limiting values at absolute zero and since it was an atomic moment (ferromagnetism) or a resultant or combination of moments (ferrimagnetisms), it was in the so called saturated condition. Having said that, there is a zero net moment in unmagnetized bulk

materials, we can predict that there will be an infinite number of degrees of magnetization between the unmagnetized and saturation conditions. These extreme situations correspond, respectively, to random orientation of domain to complete alignment in one direction with the elimination of domain walls. If we start with a demagnetized specimen and increase the magnetic field, the bulk material will be progressively magnetized by the domain dynamics described previously.

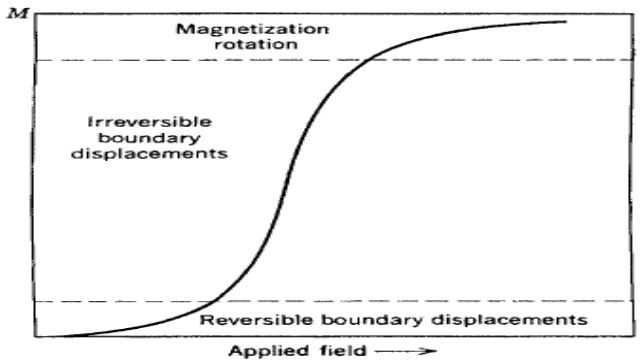

Figure 1.10 Domain dynamics during various parts of the magnetization curve

The magnetization of the sample will follow the course shown in Figure 1.10. The slope from the origin to a point on the curve or the ratio M/H has previously been defined as the magnetic susceptibility. This curve is called the magnetization curve. The curve is generally perceived as being made up of three major divisions. The lower section is called the initial susceptibility region in which there are reversible domain wall movements and rotations. Being reversible means that, after changing the magnetization slightly with an increase in field, the original magnetization condition can be returned if the field is reduced to the original value. The second stage of the magnetization curve in which the slope increases greatly is one in which irreversible domain wall motion occurs. The third section of the curve is one of irreversible domain rotations. Here, the slope is very flat indicating the large amount of energy that is required to rotate the remaining domain magnetization in line with the magnetic field.

1.4.10 Units for the Magnetization Curve

We have described the unit of magnetizing field H, from the interaction of magnetism poles. The unit was the Oersted, defined as the field experienced at a distance of 1cm

from a unit pole. We have also described the magnetic moment, ml, from the dipole. The pole density in poles per unit cross sectional area is the intensity of magnetization, M, whose units are the same as moment/unit volume = emu/cm^3.

1.4.11 Flux Lines

Faraday found it convenient to liken magnetic behaviour to a flow of endless lines of induction that indicated the direction and intensity of the flow. He called these lines flux lines and the number of lines per unit area the flux density or magnetic induction, B. The flux is composed of H lines and M lines. A schematic representation of the flux is given in Figure 1.11. Note that the lines traverse the sample, leave it at the North Pole, and return at the South Pole. In cgs units, the induction or flux density, B, is given by;

$$B=H+4\Pi M$$

A unit pole gives rise to a unit field everywhere on the surface of a sphere of unit

Figure 1.11 Magnetic flux lines composed of H (field) and M

radius. The area of this sphere is 4TC cm^2. The cgs unit of induction is the gauss. The units for the lines of induction or flux are known as Maxwell or just plain "lines". Therefore, the units for flux density, B, are Maxwell's/cm^3. B can also be Figure 1.7 Magnetic flux lines composed of H (field) and M (magnetization lines defined by the voltage generated in a wire wound around a core of magnetic material in which there are known variations of flux with time).

1.4.12 Hysteresis behaviour

In magnetic materials if we start with a demagnetized specimen and increase the magnetic field, the induction increases as shown in Figure 1.12. At high fields, the induction flattens out at a value called the saturation induction, Bs. If, after the material is saturated, the field is reduced to zero and then reversed in the opposite

direction, the original magnetization curve is not reproduced but a loop commonly called a hysteresis loop is obtained. Figure 1.12 shows such a hysteresis loop with the Initial magnetization curve and hysteresis loop magnetization curve included. The arrows show the direction of travel. We notice that there is a lag in the induction with respect to the field. This lag is called hysteresis. The area included in the hysteresis loop is a measure of the magnetic losses incurred in the cyclic magnetization process.

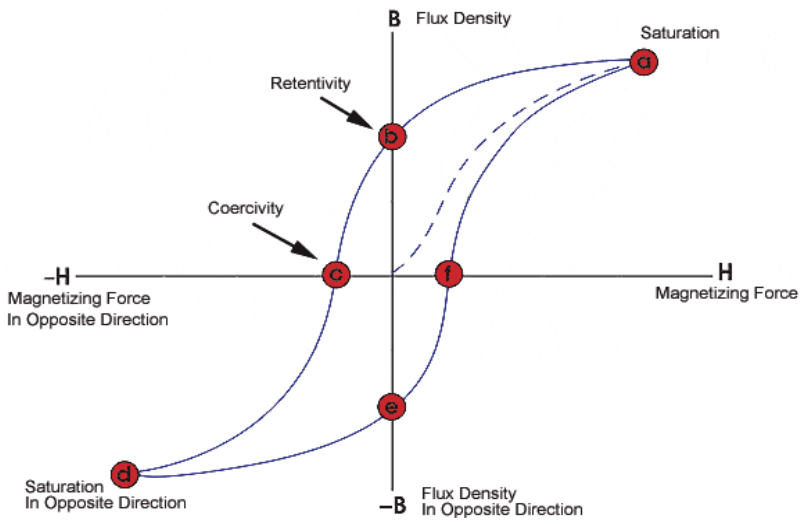

Figure 1.12 Initial magnetization curve and hysteresis loop

The value of the induction after saturation when the field is reduced to zero is called the remanent induction or remanence or retentivity, (B_r). The values of the reverse field needed after saturation to reduce the induction to zero is called the coercive force or coercivity, (H_c). Both of these properties are very important and we shall refer to them in almost every magnetic application.

CHAPTER 2
LITRATURE SURVEY

The technology of ferrites or magnetic ceramics has assumed a new importance during the last several decades and especially in the last few years. In addition to the advent of new developments such as radars, satellite communications, memory and computer applications, there has been a corresponding growth in consumer electronics markets in radio, television, power inverters etc. The most recent reason for upsurge in ferrite interest has been the development of the new, small, efficient power supplies using solid state switching, called switch mode power supplies. These power supplies are being used in computers, laptops, microprocessor, telecommunication and entertainment applications.

Figure 2.1 shows the temperature dependent magnetization in a field of 800 kA/m for the samples A, C and D. [4] These samples show close lying values of 632 ± 5 K, 627 ± 5 K and 634 ± 5 K respectively for their Curie temperature Tc, suggesting that there is no significant variation in the composition and also no size-dependent cation distribution. Similar results have been obtained by Jeyadevan et al. [5] in the case of

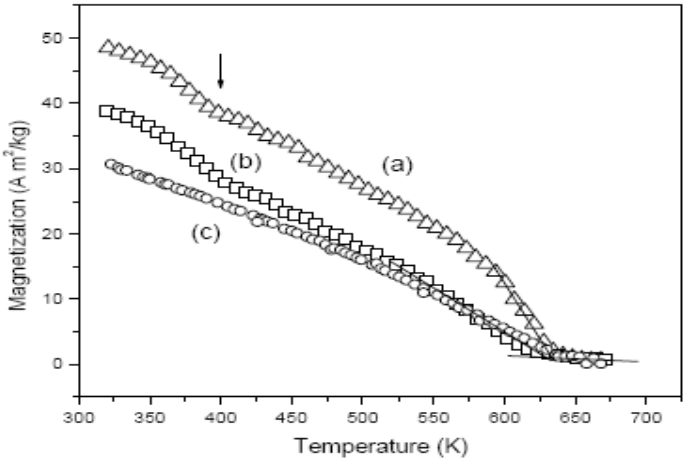

Figure 2.1. The temperature dependent of the (a) sample A, (b) sample C and (c) sample D in an applied magnetic field of 800 kA/m [4].

Mn-Zn ferrite where the Curie temperature does not change with the particle size. The bulk $Mn_{0.65}Zn_{0.35}Fe_2O_4$ shows a Curie temperature of 463 K [6] whereas the Curie temperature of the nanoparticles of this ferrite is found to be as high as 723 K, which is attributed to the redistribution of the cations among the two sites [8]. The cations

Fe^{3+},Mn^{2+} and Zn^{2+} have zero crystal field stabilization energy and hence they can occupy either tetrahedral or octahedral sites randomly. Hence the cation distribution could vary with the method of synthesis [8, 9], which explains the observed differences in the values of Tc reported in the literature [8, 10].

The heating during thermomagnetic measurements can facilitate cation redistribution and hence the metastable cation distribution in the as synthesized particles starts transforming to a thermally induced stable distribution as could be easily visualized from the change in the shape of the thermomagnetization curve (a) indicated by the arrow as in Figure 2.1. The redistribution of cations has resulted in an increase in Tc as could be visualized from the figure. The thermomagnetic measurements were also performed in a thermogravimetric analyzer (TGA) using a small horse shoe magnet with a field strength of 4 mT. Figure 2.2. (a) shows the change in the weight due to magnetization of the sample A as a function of temperature in the TGA experiment and (b) shows the second run for the same sample. The Curie temperature is found to be 634 K for the sample A. A broad hump is seen for the sample A at 520 K in the

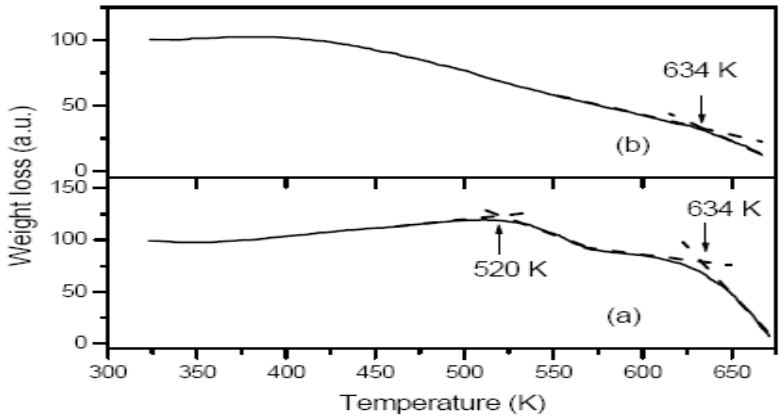

Figure 2.2 (a) The temperature dependence of magnetization of sample A measured in a TGA and (b) second run for the same sample.

virgin condition whereas the hump disappears when the sample is rerun in the TGA experiment. The small increase in the weight of the sample up to 520 K during the first run is likely to be due to the possible increase in the magnetization because of the change in the cation distribution during heating. The disappearance of the hump in the second run suggests that the cation distribution had changed from the meta-stable state to the equilibrium state on heating during the first run. The above studies suggest that, in the nano-crystalline form, the cation distribution is in the meta-stable state

whereas heating the sample takes it to the stable state. The meta-stable cation distribution is also exhibited by Mn-Zn ferrites synthesized through hydrothermal methods [8].

Jae-Man Song and Hyun-Jin Yoon and et al. [11] investigated the effect of particle size of Mn-Zn ferrite on the electromagnetic wave absorption properties in sheet-type absorbers. With increasing average particle size, the matching frequency shift toward lower frequency, and the absorption ability of the electromagnetic wave at each matching frequency decreased. However, the absorption ability increased with increasing average size of particles at 0.8 GHz and 1.8 GHz. We suggest that a sheet-type ferrite absorber with large Mn-Zn ferrite particles is useful for mobile phones. [12]

Requirements for magnetic cores used in switching power supply transformers include soft magnetism, easy magnetization with a small external magnetic field, and low loss. Magnetic materials are classified into two groups, metallic materials and oxide materials. Because the electric resistance of the metallic materials is generally lower, driving the transformer of a switching power supply causes large eddy current loss at high frequencies, typically from several ten hertz to several hundred hertz. In order to suppress loss, oxide materials, especially Mn-Zn ferrites, are used in the transformer rather than metallic materials [13]. The electromagnetic characteristics of Mn-Zn ferrite are not only dependent on the composition of the main elements but also on the material's microstructure [14]. Because of this, efforts have been made to improve their loss characteristics by controlling the size of the grains and the distribution of the small amounts of additives in the grain-boundary region [15].

In Mn-Zn ferrites the grain boundaries exhibit different chemical and physical properties than the ferrite grains. The segregation of impurities and the partial re-oxidation of the Fe^{2+} on the grain boundaries during cooling make the Mn-Zn ferrite grain boundaries highly insulating in comparison to the grain interior. These insulating layers are, in practice, very thin and therefore exhibit a relatively high electrical capacity. Core loss can be divided into three components: hysteresis loss , eddy-current loss and residual loss . The proportions of these components in the total loss can vary widely, depending on the measurement conditions such as frequency and magnetic flux density. At low frequencies, hysteresis losses are dominant, and in

order to reduce these losses it is important to form a uniform microstructure that is free from lattice defects and pores. At high frequencies, the proportion of eddy current losses increases, but this can be reduced by increasing the resistance of the cores. Eddy current loss can be decreased by having grain boundaries with a high electrical resistance and by having a ceramic microstructure with small grains. The resistance of the grain boundaries is determined by additives which are enriched at the grain boundaries during the sintering process, forming an insulating phase. Small grains can be achieved by applying sintering conditions that suppress the grain growth and by choosing additives that act as grain growth inhibitors. The sintering parameters must lead to a suppression of the grain growth. Therefore, the choice of raw materials, as well as the technological parameters, influences the power losses. In general, two extreme cases regarding the eddy current in the magnetic core of Mn-Zn ferrites can be identified by applying the brick-wall model [16].

According to Stoppels [17], miniaturization of electronic devices has lead to the increase in driving frequency to more than 1 MHz and at this high frequency level the power loss dramatically increases, fostering the development of new low-loss materials. The main contributions to the total loss are hysteresis, eddy current and residual losses respectively which predominate at different frequencies. A fine-grained homogeneous microstructure with highly resistive grain boundaries is required to minimize eddy current losses at intermediate and high frequencies.

Akashi [18] showed that the simultaneous addition of CaO and SiO_2 to Mn-Zn ferrites made electrical resistivity higher and improved magnetic properties. The additives of CaO and SiO_2 were reported to concentrate around the grain boundaries to form a highly resistive layer. The thickness of the layer was reported to be 1-5 nm and was dependent on the quantity of the additives of CaO and SiO_2, sintering temperature and the heating rate of sintering. It was further reported by Tsunekawa et al [19] that a large distortion of the spinel lattice near the grain boundaries occurred due to the incorporation of Ca atoms in the spinel lattice and produced deleterious effect on the power loss property of the Mn-Zn Ferrites.

Znidarsic et al [20] reported the effect of Ta_2O_5 in lowering the power loss at high frequencies in Mn-Zn ferrites. Ta_2O_5 was reported to inhibit the grain growth and increased electrical resistivity by segregating at the grain boundaries.

For obtaining high magnetic permeability the presence of grain boundaries will act as impediment to domain wall motion. The fewer the number of grain boundaries present, the larger the grains and higher the permeability. In ferrites where the grain boundaries are thicker, same unhindered movement does not occur. The lack of purification scheme in processing, the presence of pores and inclusions, as well as greater chemical inhomogeneity prevent the attainment of high permeability. [21]
The relationship between grain size and permeability will generally be linear only if the grain growth is normal, that is if all grains grow pretty much at same time and same rate. This leads to rather narrow range of the final grain sizes. If, indeed, some grains grew very rapidly they would trap pores, which can limit permeability by pinning domain walls. When conditions permits this kind of grain growth to occur, with many included interagranular pores it is called exaggerated or discontinuous grain growth.

Drofenik (1985) [22] has reported that distance between pores rather than grain size account for variations in permeability. Samples with gaint grains and included porosity owing to exaggerated grain growth still had higher permeabilities than those with normally grown grains, provided the distance between the pores were the same. Drofenik [22] concluded that the large grained samples are less sensitive to grain boundary effects, and thus the μ versus T curve is more peaked.

Reoess (1971) [23] has reported that the ferrite is an undesirable type of microstructure that lowers the permeability and increases the losses. This type of structure has very large grains in the matrix of the fine grains. It is most often due to the segregation of a particular impurity such as SiO_2 which produces the rapid grain growth locally while other undoped areas are unaffected. (Yoneda, 1980), [24]

Porosity is the microstructural feature limiting the movement of domain walls. Pores and other imperfections would appear to pin walls especially within the grain

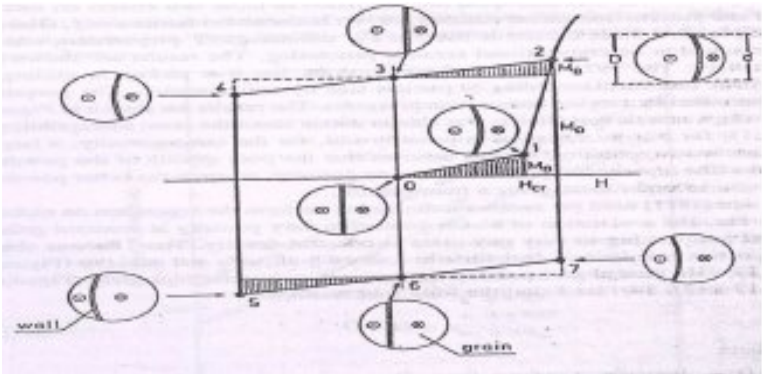

MB = bugling Magnetisation MD = Displacement Magnetisation

Figure 2.3: magnetization of ferrites showing the domain wall bugling and displacement

Globus (1972)[25] however , pointed out that domain wall bugling would still permit wall movement even while the end points were tied down. The mechanism illustrated in the figure shows that, the growing of large grains in ferrite creates a problem: many pores are swept over by the grain boundary and remain within the large grains. Intragranular porosity is more deleterious than intergranular porosity.

Influence of particle size on the magnetic properties of polymer bonded NdFeB magnets was studied by A. Handstein, K.H. Muller, R. Grossinger, H.R. Kirchmayr and R. Krewenka in 1991[26]. They studied that particle size in polymer bonded NdFeB magnets has a remarkable influence on the magnetic properties. The difference is caused by the oxygen content of the powder. Different fractions of particle size obtained by sieving of original and milled MQI- powders were used for preparing bonded magnets were used. The coercivity of compacted powders prepared by milling of melted ingots increases with decreasing particle size. The oxygen content increases monotonously with decreasing particle size. The smaller the particles made from flakes the smaller the nucleation fields for demagnetization modes in the particles. In all cases the increasing oxygen content is accompanied by decrease of remanence.

Manganese-zinc ferrite ($Mn_{0.52}Zn_{0.41}Fe_{2.07}O_4$) has been prepared by the mixed-oxide route. Specimens were in the form of toroids pressed in the green state to 11.9 mm outside diameter and 5.9 mm inside diameter. To assess the effect of zinc loss, a variety of circular local sintering enclosures were employed. All specimens were

initially sintered in air at 1390°C for times of 7.5-16 h. After cooling to 1200°C they were held for 4 h in atmospheres containing 0.0125-0.05% oxygen. Sintered products were single-phase, with density greater than to 95% theoretical and a grain size of about 20μm. Use of a partial sintering enclosure led to a 45% increase in initial permeability μ_i, but use of a full enclosure led to a reduction in μ_i. Firing the samples at 1200°C in an atmosphere containing initial permeability was maximized (about 10200) over a wide range of temperatures 25-90°C. The eddy current losses in such samples were twice as high as for samples sintered in an oxygen atmosphere containing 0.05% oxygen [27]

Mn-Zn ferrite cores having grain size of about 8~10 μm were produced by controlling the calcination temperature, after calcinations milling time and sintering conditions. The ferrite powder production conditions and core microstructure were examined to determine their effects on the magnetic properties and mechanical strength of Mn-Zn ferrite cores. A tendency of core loss to decline with a decrease in grain size was confirmed. Strength increased also with a decrease in grain size. Thus a relation similar to that between strength and fracture toughness in the equation of Griffith-Irwin was noted. By these findings, it has become possible to produce Mn-Zn ferrite cores with lower loss and greater strength. [28]

CHAPTER 3
EXPERIMENTAL WORK

This chapter highlights the experimental work carried out in different stages of the project, which involves

- Preparation of Ferrite powder and its characterization.
- Forming powder into cores.
- Firing or Sintering.
- Characterization and testing of cores.

All the steps involved in the ferrite synthesis are given in a nutshell in the flow chart in figure 3.1. Each step is discussed in detail in the following paragraphs.

3.1 Powder Preparation

The ferrite powders were produced by conventional ceramic processing technique, which is one of the most critical steps that control the electrical and magnetic properties of the finally obtained ferrite cores. It consisted of following steps:

3.1.1 Dry Mixing

High purity raw materials of the basic composition 51.96 mole% ferric oxide (99.8% Purity), 37.88 mole% manganese oxide (99% purity) and remaining 10.16 mole% zinc Oxide (99.5% purity), were mixed and blended homogenously through dry mixing in the pot mill for few hours.

3.1.2 Calcination

Homogenously blend of raw material mixture is further exposed to temperature of 950^{o}C for 90 minutes in air atmosphere in the rotary kiln furnace. The purpose of calcining is to start the process of forming of spinel ferrite lattice. This process is essentially one of inter-diffusing phenomenon of substituent oxides into a chemically and crystallographically uniform structure. The driving force for the inter diffusion is the temperature and concentration gradient. As the individual oxides inter-diffuse, some ferrite is created at the interface. This complete phase reduces further diffusion because the concentration gradient is no longer present to act as a driving force. The material in the centre of each oxide particles remains as such, as they experience the

difficulty in diffusing through the ferrite since the diffusion distance becomes larger. Since some shrinkage occurs in calcining, one advantage of the process is to reduce the shrinkage in the final sintering. This allows better control of the final dimension of the sintered core. In addition, calcining helps in evaporation of the volatile impurities and homogenization of the powder mixture. During this process, the powder coarsens considerably, and the colour changes from red to grey or black. The degree of calcining action, or in other words spinel formation can be studied from the X-ray Diffraction (XRD) pattern. It shows the peaks of spinel phase formed and the unreacted residual Fe_2O_3 or hematite phase.

3.1.3 Milling

After calcining, the material is broken up by ball milling and attrition action. The particle size reduction is carried out to achieve the desired specific surface area (SSA) of 5500-5600 cm^2/gm through ball milling with 32 mm steel balls followed by fine milling in attritor with 6 mm steel balls. The amount of milling determine the particle size distribution, which in turn influence the homogeneity of the compact going into the final firing as well as the microstructure after the sintering process. In the mid-stage of milling, high purity additives such as calcium oxide, zirconium oxide, niobium oxide, bismuth oxide etc in desired quantity are added to the slurry in the ball mill. Specific surface area (SSA) is measured through Blains apparatus.

3.1.4 Drying and Granulation

Slurry obtained after milling is then dried in the oven, so as to remove the moisture and obtain a press-able powder. Organic additives such as Polyvinyl Alcohol (PVA) and Polyethylene glycol (PEG) are employed to facilitate this step. PVA is added as a binder to provide green strength to the pressed compact [29], so that it can be handled easily in the green stage for further processing, PEG acts as a plasticizer so as to soften the particles [30].

The mixture of PVA, PEG and dried slurry is than granulated in the agate mortar, so as to obtain free flowing granulates. The granules are classified by mechanical sieving and the fraction between 200 and 500 μm are subsequently used for pressing.

FLOW DIAGRAM OF FERRITE MANUFACTURING

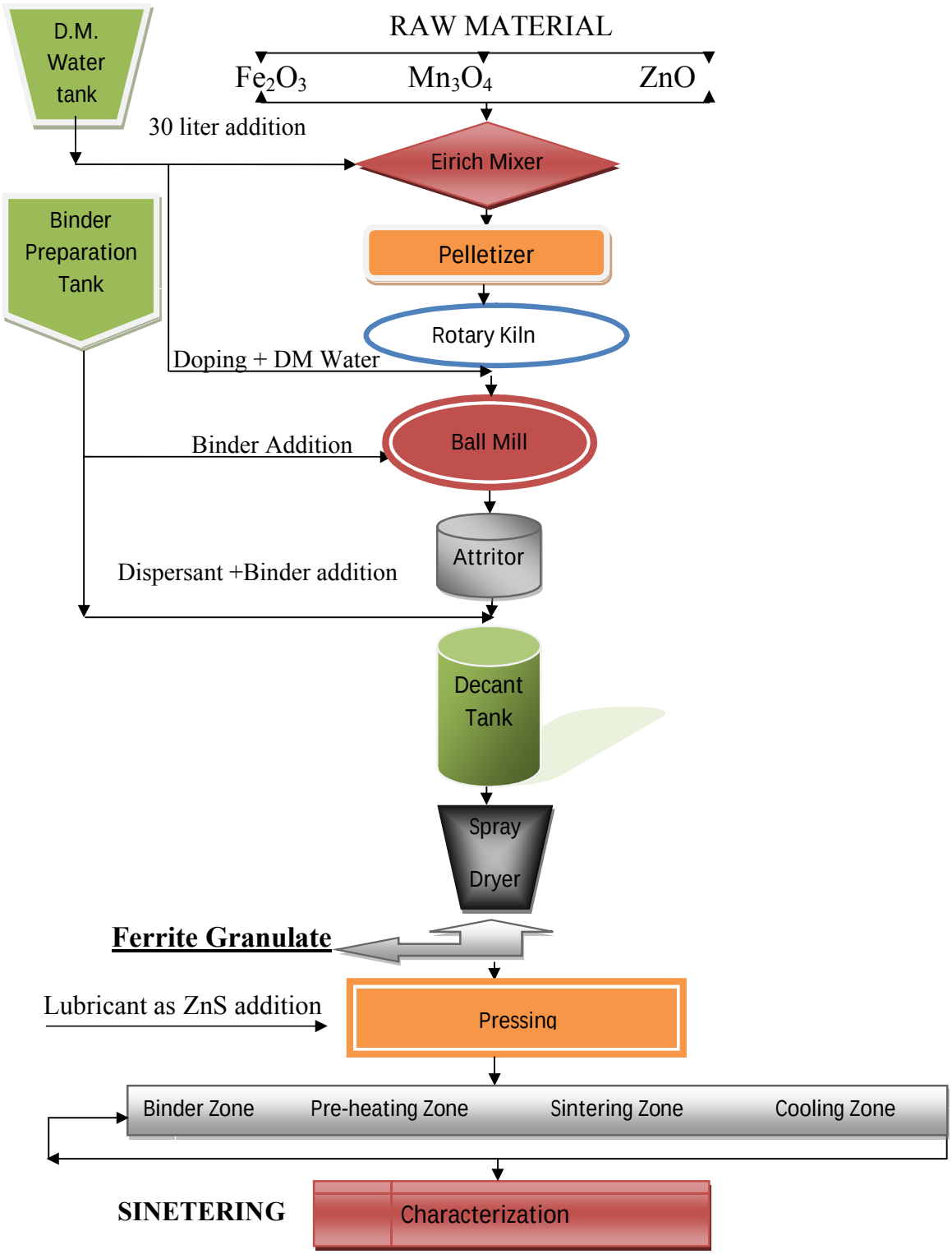

Figure3.1 Flow sheet for the synthesis of sintered Manganese Zinc Ferrites.

3.2 Forming

The second step in the ferrite processing technology is the forming of the components. In this step, dry pressing of granulates into the toroid core configuration is carried out. Dry pressing or compacting is done in a mechanical press using a combined action of top and bottom punches in a cavity such that toroids of external diameter of 29.13 to 29.20 mm, internal diameter of 17.38 to 17.45 mm and height of 14.17 to 14.25 mm is obtained. In this process toroid cores with the green density of 3 to 3.2 gm/mm^3 are obtained Figure 3.2 below shows some of the aspects of die pressing. Before proceeding for dry pressing, granulates are treated with external lubricants such as zinc stearate, which produces a coating of fine lubricant particles on granule surface, as shown in figure 3.3 taken from literature. [31]

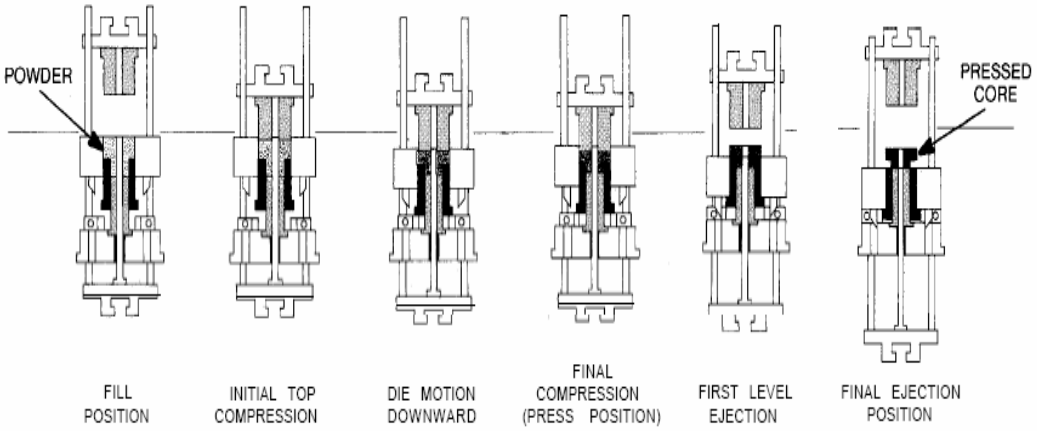

Figure 3.2- Dry pressing techniques

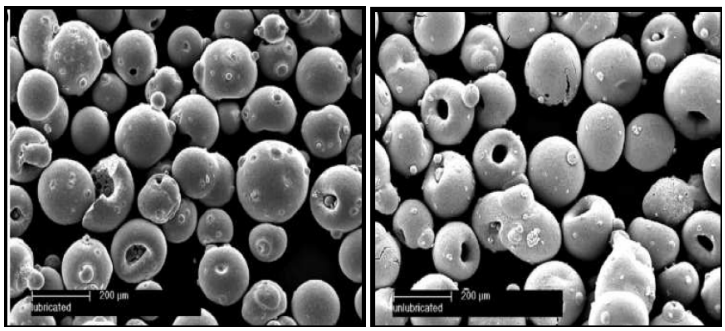

Figure 3.3- Scanning electron micrographs of granules (a) with external lubricant and (b) without external lubricant. [31]

External lubricants also serve to lubricate the die and punch surfaces. The addition of external lubricant increases tool life [31] and helps produce a uniform green body. In addition to providing die-wall lubrication, external lubricants can improve the flow properties of granulated powder by reducing inter-granular friction and hence fill the die more efficiently. Improved packing characteristics can eliminate large inter-granular voids and hence contribute to a low porosity microstructure of the final sintered ferrite core.

3.3 Sintering

This is the most critical step in the ferrite processing. It is during this phase of the process that the product achieves its final electric, magnetic and mechanical characteristics. Sintering of manganese-zinc ferrites requires equilibrium between time, temperature and atmosphere along each step of the sintering cycle. Sintering starts with a gradual ramping up from room temperature to approximately 900^{o}C as impurities, residual moisture, binders (PVA, PEG), and lubricants (Zinc stearate) are burned out of the product.

The atmosphere in this part of the sintering cycle is 20% oxygen (complete air). The temperature is further increased to the final sinter temperature of 1320^{o}C at high heating rate. While the temperature is increasing, nitrogen gas is introduced into the kiln and the partial pressure of oxygen is maintained at 5% at the sintering temperature of the kiln atmosphere.

During the cool-down cycle a reduction of oxygen pressure is very critical in obtaining high quality Mn-Zn ferrites and so the oxygen partial pressure is dropped down to ppm level. Sintering of the green toroid samples is carried out in programmable Linn batch kiln. Firing schedules and equilibrium oxygen partial pressure conditions maintained are indicated in the sintering profile in below table 3.1 Figure 3.4 shows the typical sintering profile carried out in this thesis.

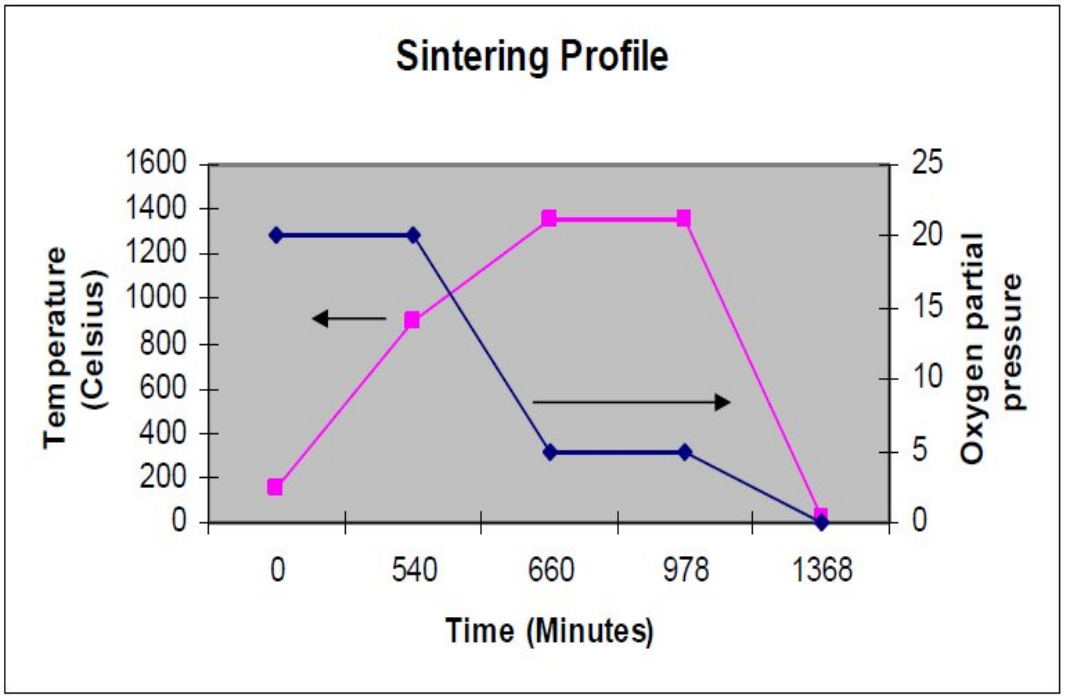

Figure 3.4 Schematic Diagram of the atmosphere and temperature profiles used during sintering.

Table 3.1 Typical Sintering Profile.

Sintering profile			
Time Hrs	**Time (Min)**	**Temp (^{o}c)**	**Oxygen (%)**
0	0	150	20
9	540	900	20
11	660	1320	5
15.3	978	1320	5
22.8	1368	25	0.01

3.4Characterization

Detailed studies of the Magnetic properties of ferrite samples were carried out. Samples were also put to phase analysis and microstructural characterization.

3.4.1 Specific Surface Area

Specific Surface area is material property of solids which measures the total surface area per unit of mass [35], solid or bulk volume [36] or cross section area. It is a derived scientific value that can be used to determine the type and properties of a material. It is defined either by surface area divided by mass (with units of m^2/kg), or surface area divided by the volume (units of m^2/m^3 or m^{-1}) It has a particular importance in case of adsorption, heterogeneous catalysis and reactions on surfaces

$$SSA = K.\ (t)^{½}\ cm^{2}/gm$$

Where K = Standard SSA/ (Blain time in second)

t= Blain time in second

3.4.2 Electrical and Magnetic Characterization

The measurement of Inductance factor (AL) and Inductance (LS) of each sintered toroid was carried out using Hewlett Packard multi-frequency LCR meter (model no.-4275A), and other properties such as initial permeability were derived using the mathematical relations mentioned in the literature. Inductance Factor AL (nH), which is the inductance of the coil on the specified core divided by the square of the number of turns, was directly measured through LCR meter under test conditions, of frequency of 10 KHz and voltage of 150mV, by putting the probes at the centre of each toroid sample. The resistance of the ferrite core was measured by putting the probes of the multi-meter at the two specific points on the ferrite core. For measuring the Inductance value, the toroid samples were properly wound with the copper wire with 20 turns and the measurements were carried out using LCR meter at the test conditions of frequency set at 10 KHz and voltage of 0.005 Volts. Initial permeability (μ_i) of the toroid samples with 20 turns in the coil were calculated using the inductance value in the below mentioned mathematical relation [1].

$$\mu_I = [4\pi\ LS / h\ \ln(D1/D2)] \qquad (1)$$

Where h represents the width of the core, D1 and D2 are outer and inner diameters of the Toroid core respectively. Variation of initial permeability with temperature was

studied using the Curie set up consisting of a wound ferrite sample dipped in the silicon oil containing flask placed over a heater. The ferrite core is uniformly heated at a constant heating rate and the Inductance value corresponding to the temperature is measured by LCR meter. Initial permeability was calculated according to equation (1) and its value is plotted against temperature. Due to the limitations of the available apparatus, Curie temperature of the samples was not measured. Variation in Initial permeability with frequency is measured similarly through LCR meter and plotted. Power loss characteristics and magnetic flux density B_{max} of the ferrite samples were studied using power loss analysis set up consisting of Signal generator (Model-FG2002C), Power amplifier (Model no.-EV- 300/F) and Norma AC/DC Power analyzer (Model no.-D5245). Power loss was measured under the conditions of 100 KHz /100 mT and 100 KHz /200mT, Bmax was measured at the frequency 16 KHz, and magnetic field of 250 Amp/m. Variation in power loss and B_{max} with temperature was studied by placing the test samples in the dry heating chamber. Temperature in the heating chamber was varied by the interval of 10 ^{0}C up to 130 ^{0}C and corresponding variation in above mentioned properties was measured.

3.4.3 Thermo gravimetric Analysis (TGA)

The behaviour of the ready to press granulates under increasing temperature was studied through thermo-gravimetric analysis. The analysis was done in the nitrogen buffer at the temperature of 600 and 1100^{o}C at the rate of 10^{o}C/min and 20^{o}C/min respectively. The weight of the samples was recorded as the function of the increasing temperature. TGA plot gives the clear knowledge about the binder burn out region in the sintering zone.

3.4.4 X-Ray Diffraction (XRD)

XRD analysis of the calcined powder and sintered crush powder is done to study the ferrite phase formation.

3.4.5 Microstructural Study

The microstructure of well-ground and polished sintered specimen was studied by Optical Microscopy using Nikon optical microscope. The samples were etched with Hydrofluoric acid for 2 minutes.

CHAPTER 4

RESULTS AND DISCUSSION

The synthesized ferrite powders and sintered ferrite samples were characterized following the procedure mentioned in Chapter-3. Before doing instrumental characterization, powders were visually inspected. Spinel powders were dark grayish/blackish in colour. When brought nearer to a permanent magnet, they were strongly attracted to the magnet, suggesting ferrite formation. In this chapter, results obtained from the characterizations are discussed.

Table 4.1 Composition of low power loss Mn-Zn ferrites material

Raw Material *	Amount (mole %)	Purity (%)
Ferric Oxide (Fe_2O_3)	51.96	99.8
Manganese Oxide (Mn_3O_4)	37.88	99
Zinc Oxide (ZnO)	10.16	99.5

* Moisture of raw materials = (0.1-0.3) %

Table 4.2 Dopent used in low power loss Mn-Zn ferrite

Dopant Name	Amount (ppm)
CaO	500
Bi_2O_3	150
Nb_2O_5	300

Table 4.3 Binder (Polyvinyl Alcohol) used in Mn-Zn Ferrite

Sample Number	Amount (mole %)
A	0.4
B	0.8
C	1.0

Plasticizer- Polyethylene Glycol

Lubricant- Zinc Stearate

Table 4.4 Composition of High Initial Permeability Mn-Zn ferrites material

Raw Material	Amount (mole %)	Purity (%)
Ferric Oxide (Fe_2O_3)	50.78	99.8
Manganese Oxide (Mn_3O_4)	27.18	99
Zinc Oxide (ZnO)	22.04	99.5

Table 4.5 Dopent high Initial Permeability Mn-Zn ferrites material

Dopant Name	Amount (ppm)
Bismuth Oxide	200

Test Sample: From the entire each five samples for testing of electrical and magnetic property of low power loss and high initial permeability Mn-Zn ferrite material at different milling time of attritor {table 4.8(composition-table 4.1and 4.2) and 4.10(composition-4.4 and 4.5)} were taken.

4.1 Specific Surface Area

Specific surface area of Mn-Zn Ferrite shows in table 4.6 with different milling time of ball mill and attritor.

Table 4.6 Value of SSA and milling time of Mn-Zn Ferrite powder

Time (Hrs.)	TYPE	SSA	Difference	Time (Gap)	cm^2/min. Increasing
1	Ball Milling SSA	3699	0	1	0
2		3733	34	1	0.57
3		3791	58	1	0.97
4		3791	0	1	0.00
5		3791	0	1	0.00
1	Attritor SSA	4296	505	1	8.42
2		4536	240	1	4.00
3		4665	129	1	2.15
4		4886	221	1	3.68
5		5048	162	1	2.70
6		5246	198	1	3.30
7		5302	56	1	0.93
8		5349	47	1	0.78

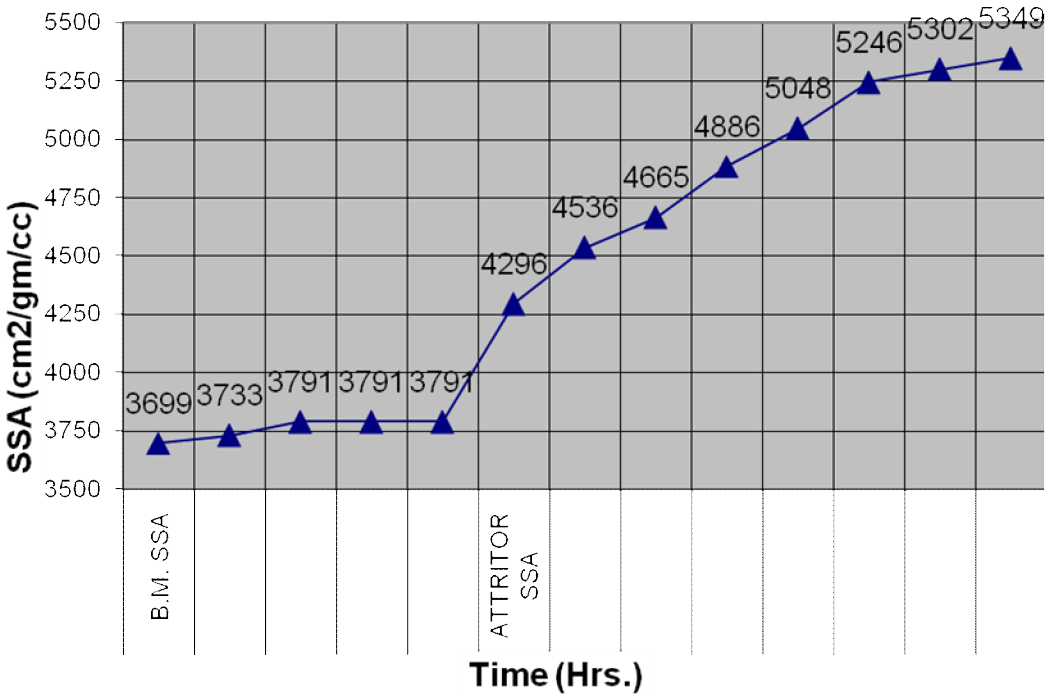

Figure 4.1 Variation of specific surface area with milling time of Mn-Zn Ferrite (trial-1)

Table 4.7- Value of specific surface area and milling time of Mn-Zn ferrite powder

Time (Hrs.)	TYPE	SSA	Difference	Time (Gap)	cm^2/min. Increasing
1	B.M. SSA	3634	0	1	0
2		3669	35	1	0.58
3		3646	-23	1	-0.38
4		3794	148	1	2.47
5		3726	-68	1	-1.13
1	ATTRITOR SSA	4711	985	1	16.42
2		5006	295	1	4.92
3		5064	58	1	0.97
4		5339	275	1	4.58
5		5440	101	1	1.68
6		5653	213	1	3.55
7		5763	110	1	1.83

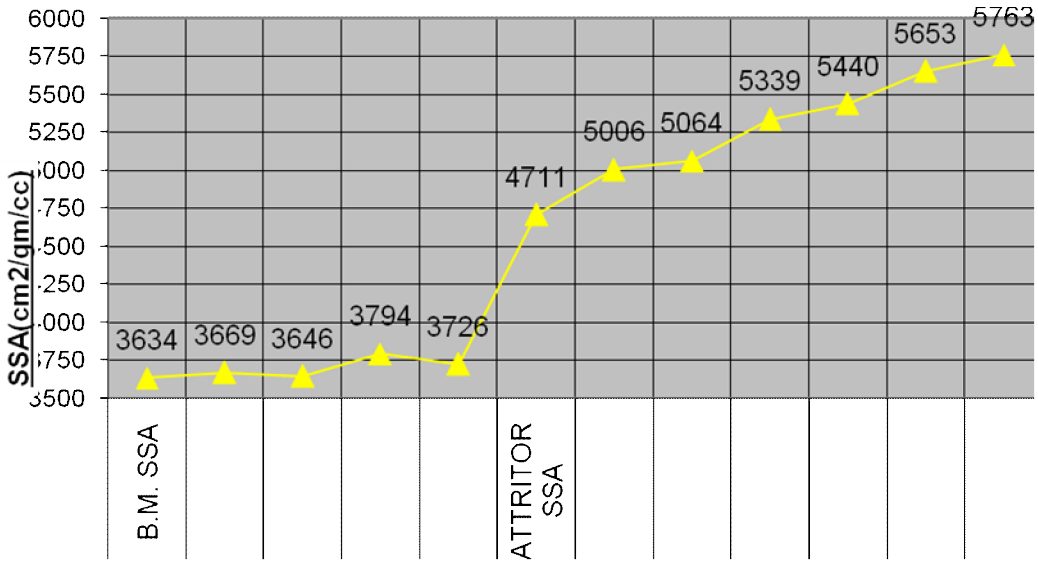

Figure 4.2 Variation of specific surface area with milling time of Mn-Zn Ferrite (trial-2).

According to above graphs between SSA and time we can say that we can reduce the ball milling time for maintaining required SSA can be reduced. According to figure 4.1 and 4.2 no more change in SSA during 3-5 Hrs because collision between ball and particle will be low.

Here we maintain SSA for achieving better electrical and magnetic property of the ferrites core. The bonding will be proper and spinal phase formed easily which gives better property. In ball milling, the ratio of crushing of granules becomes constant so not showing more variation in SSA. The rate of crushing depends on mill parameter (Diameter, Speed & amount of media) and properties of grinding media (Size, shape and hardness) the rate of crushing depends on the number of contact points between the ball and sintered pallets and that the number of contact points in turns depend on surface area of balls, the rate of grinding will increase inversely as the radius of the balls. The rate of grinding also depends on particle size. The rate decrease with decreasing particle size and as grinding process. [37]

4.2Electrical and Magnetic Properties

Manganese-Zinc ferrite samples synthesized in this work was tested for their electrical and magnetic properties. Its magnetic properties are dependent on many factors, e.g. pressure, particle size and magnetic field intensity. To achieve magnetic properties in the spinel ferrites it is necessary to consider the anisotropic energies which are related to the crystal structure and microstructure of the materials. This anisotropic energy is controlled through macroscopic property of magnetic material. They are respectively (a) the magnetocrystalline anisotropy energy which favour spin alignment in an easy crystalline direction, (b) the magnetostructive energy related to strain anisotropy, (c) the magnetostatic energy related to shape anisotropy. Toroid shape is selected for magnetic components because of their ability to minimize demagnetizing or fringing field which would otherwise represent an energy loss to the system.

The magnetocrystalline anisotropy is that part of crystal energy which is dependent on the direction of magnetization in the lattice and

$$Ea = K_0 + K_1 (\alpha_1^2\alpha_2^2+\alpha_1^2\alpha_3^2+\alpha_2^2\alpha_3^2) + K_2 (\alpha_1^2\alpha_2^2\alpha_3^2) + \ldots\ldots\ldots\ldots\ldots\ldots\ldots\ldots$$

Where α_1, α_2, α_3 are direction cosine of magnetization with respect to the cubic axis of the crystal. K_0 is anisotropic constant, K_1 value of minimum energy position an arbitrary constant, K_2 & K_3 are an isotropic constant of the [110] and [111] direction. The anisotropic constant is different from on a material to another and is also temperature drop. The magnetocrystalline anisotropy is dependent on K1, the first order anisotropy constant and is strongly influenced by cation present in the crystal structure in Mn-Zn ferrite system. There is a little contribution to K_1 by Mn^2+ while Fe^{3+} Ion has a slight positive contribution because of temperature dependent of this effect. It is possible to have a net zero anisotropy value at some temperature. Material temperature coincides with well known secondary maximum in magnetic permeability. The application of spinel ferrites depends on achieving high permeability, low coercive force and low hysteresis losses, consequently, the strong effect of divalent iron places stringent requirement on the composition and processing of spinel ferrites. The outcome of the electrical and magnetic characterization of the samples is discussed in the following paragraphs.

4.2.1 Power Loss Characteristics

Power loss density (Pv) and magnetic flux density (B_{max}) of the ferrite samples were measured through power loss set up as mentioned in the preceding chapter. Power loss was measured under the conditions of 100 kHz/100mT and 100 kHz/200mT for each sample, Magnetic flux density B_{max} was measured at the frequency of 16 kHz and magnetic field strength of 250 A/m. The values of the measured properties are mentioned in table 4.8.

Table 4.8- Value of power loss and magnetic flux density for low power loss Mn-Zn ferrite samples

Sample	SSA (cm^2/gram)	Temperature	Power Loss 100Khz/100mT	Power Loss 100khz/200mT	B-max 16khz/250A/M	B-max 10khz/1000A/m
1	3044	25^0C	217	991	444	497
		100^0C	113	685	383	435
2	4306	25^0C	187	868	451	501
		100^0C	92	566	396	438
4	4878	25^0C	161	164	458	505
		100^0C	75	468	402	438
6	5169	25^0C	153	699	472	517
		100^0C	69	416	416	450
8	5468	25^0C	160	760	479	529
		100^0C	74	471	424	461

The power loss analysis data of ferrite samples as shown in table reveal a substantial variation in power loss with specific surface area.

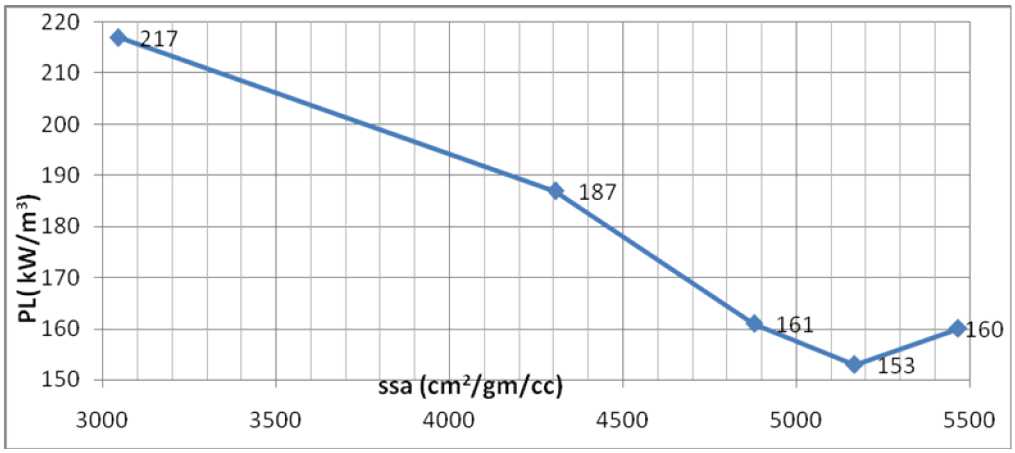

Figure 4.3 Variations in Power Loss at 25^{0}C at 100 kHz and 100mT with specific surface area

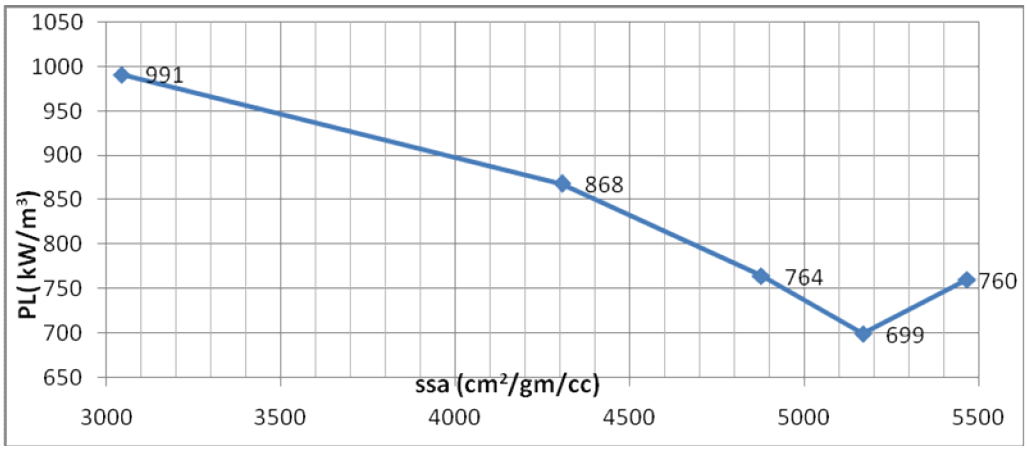

Figure 4.4 Variations in Power Loss at 25^{0}C, 100 kHz and 200mT with specific surface area

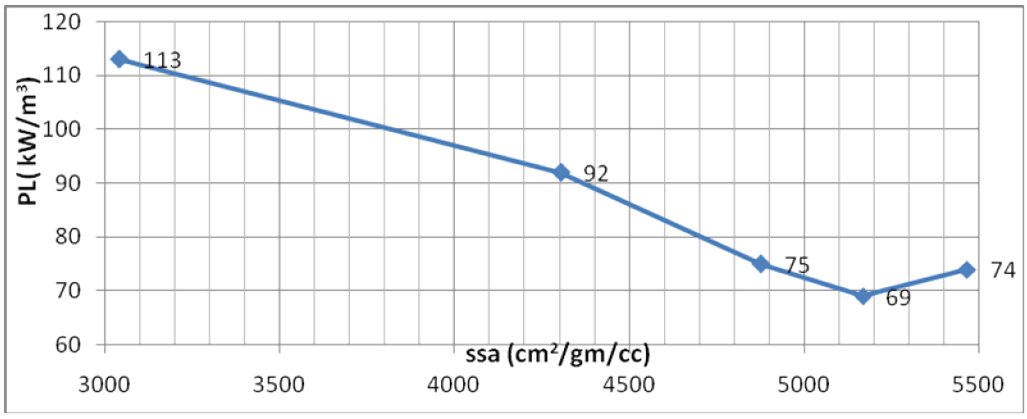

Figure 4.5 Variations in Power loss at 100 ^{0}C 100kHz and 100 mT with specific surface area

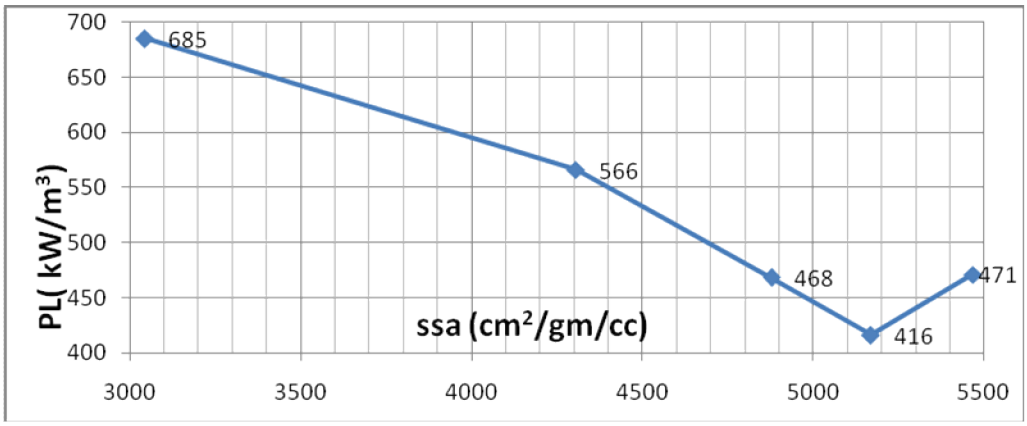

Figure 4.6 Variations in power loss at 100 ^{0}C 100kHz and 200mT with specific surface area

Figure shows the variation in total power loss at 100 KHz / 200mT as a function of SSA of Mn-Zn ferrite powder. At SSA 5169 cm^2/gm power loss is at lowest after that power loss is increasing for Mn-Zn ferrite. At this point compaction will be proper and phase formed in sintering will obtain spinal structure. The water absorbance, porosity and structure change with SSA. Power loss also depends on temperature, frequency and dopants.

4.2.2Magnetic flux density

Variation in Magnetic flux density of the samples with temperature measured under the conditions of 16 KHz frequency and applied magnetic field of 250 A/m is plotted in the figure 4.7-4.10 below. A slight increase though random, is observed in the samples with SSA.

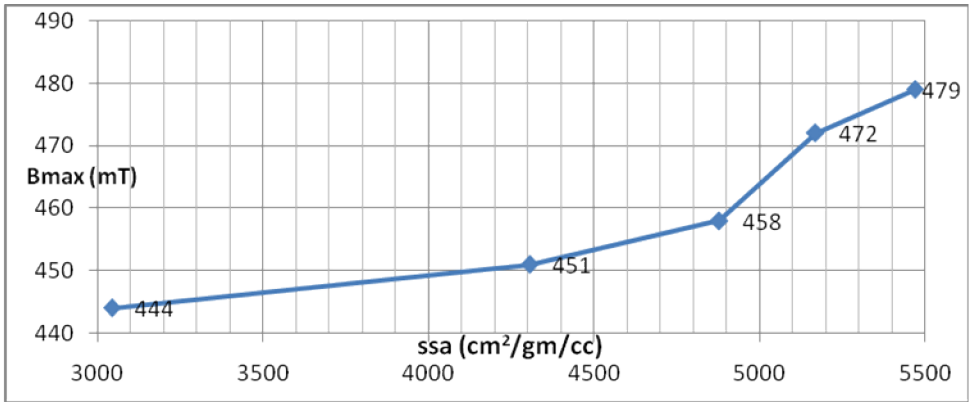

Figure 4.7 magnetic flux density at 25 ^{0}C, 16 kHz and 250A/M with specific surface area

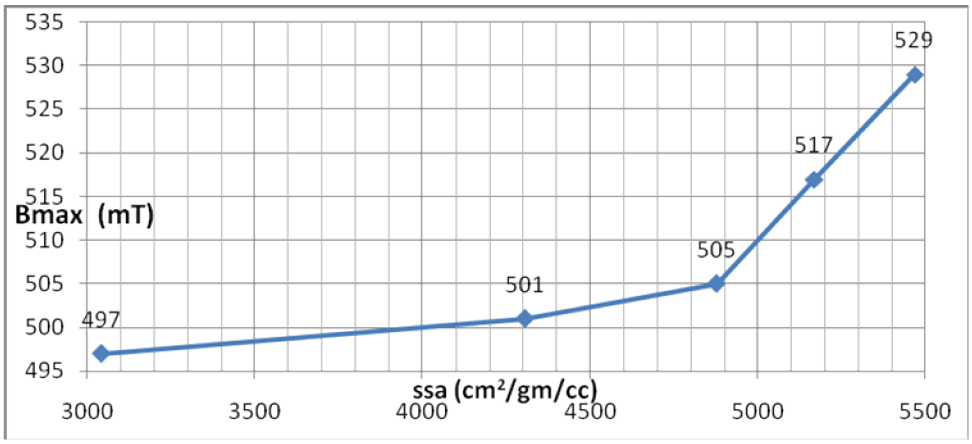

Figure 4.8 magnetic flux density at 25 ^{0}C, 10 kHz and 1000 A/m with specific surface area

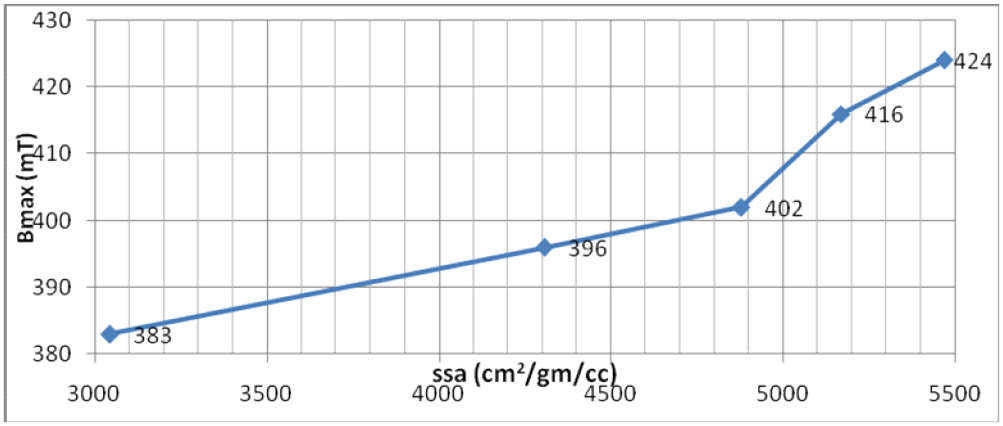

Figure 4.9 magnetic flux density at 100^{0}C16 kHz and 250 A/m with specific surface area

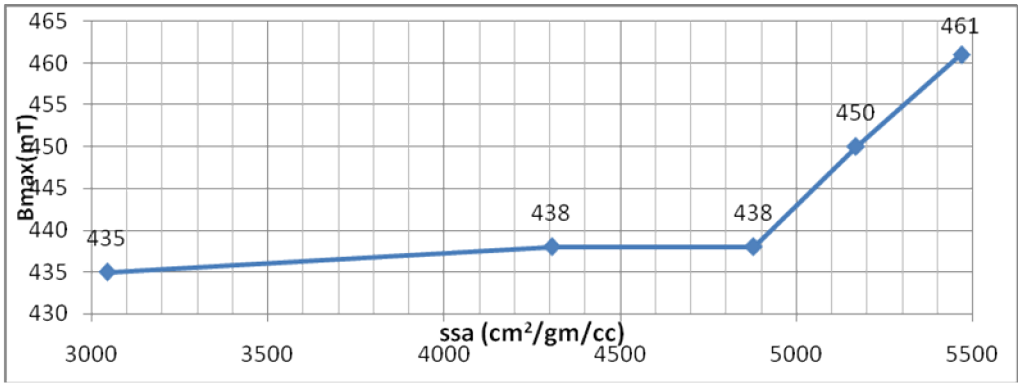

Figure 4.10 magnetic flux density at 100^{0}C 10 kHz and 1000A/m with specific surface area

When the nonmagnetic zinc ion is substituted into a magnetic ferrite lattice, it has a stronger preference for the tetrahedral site than does the ferric ion and thus reduces the amount of Fe^{3+}, on the A site because of antiferromagnetic coupling, the net result is an increase in magnetic moment on B lattice and an increase in increase in saturation magnetization. At large levels of Zn substitution the A site magnetic ion becomes so diluted that the coupling between the two lattices is lost and the saturation magnetization drops. An additional consequence of the weak magnetic interaction is that they can be disrupted by thermal energy so that the temperatures at which the magnetic property disappear (Tc) decrease with increase Zn content.

4.2.3 Inductance factor and Resistance

Inductance factor (AL), Resistance (R) and Initial permeability of the Mn-Zn ferrite samples prepared in this work measured under the specific conditions discussed previous chapter.

Table 4.9 Value of inductance factor and resistance

Sample	**ssa (cm^2/gm/cc)**	Inductance Factor (µH)	Resistance (ohm)
1	3044	1850	62
2	4306	1979	70
4	4878	1990	46
6	5169	2160	37
8	5468	2031	73

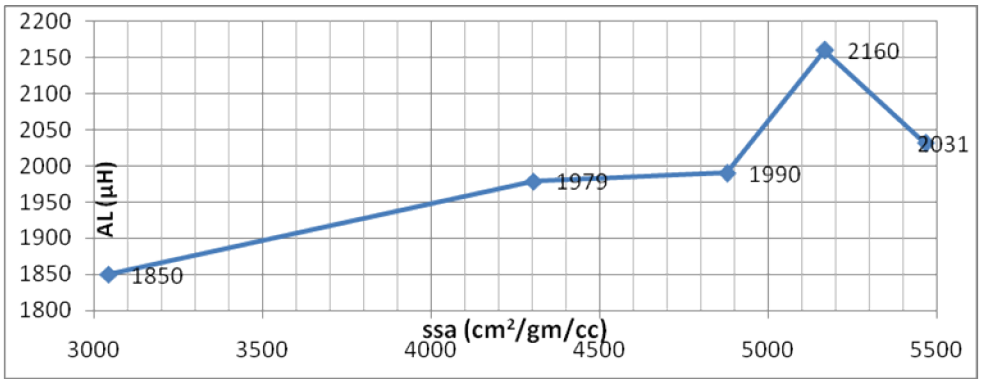

Figure 4.11 Variation in inductance factor with specific surface area

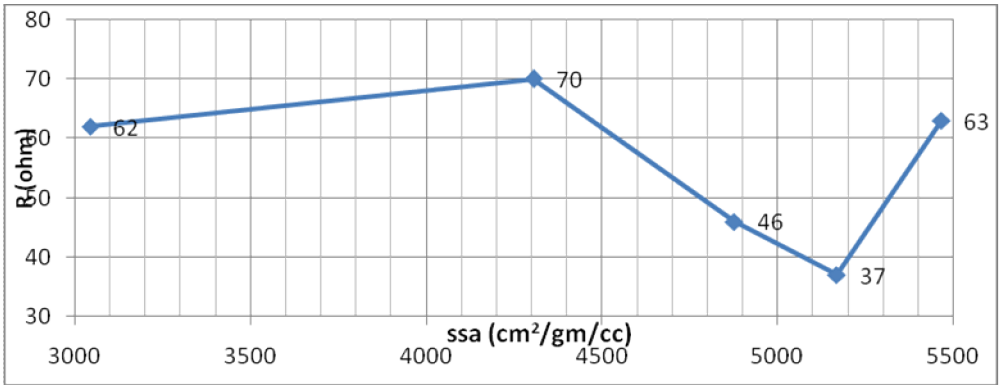

Figure 4.12 the variation in Resistance (R) with specific surface area of Mn-Zn Ferrite powder

4.2.4 Initial permeability and Quality Factor

Table 4.10 shows the value of Initial permeability (μ_i) and Quality factor (Q) of high magnetic permeability Mn-Zn ferrite material.

Table 4.10 value of μ_i, Q at 10 kHz and 100 kHz with variation in specific surface area

Sample	**ssa (cm^2/gm/cc)**	Initial Permeability at 10 kHz	Initial Permeability at 100kHz	Quality factor(Q)
1	4341	5504	5021	3.5
2	4964	7764	6644	2.59
4	5248	8126	6964	2.58
6	5359	8960	7739	2.54
7	5562	7906	6917	2.57

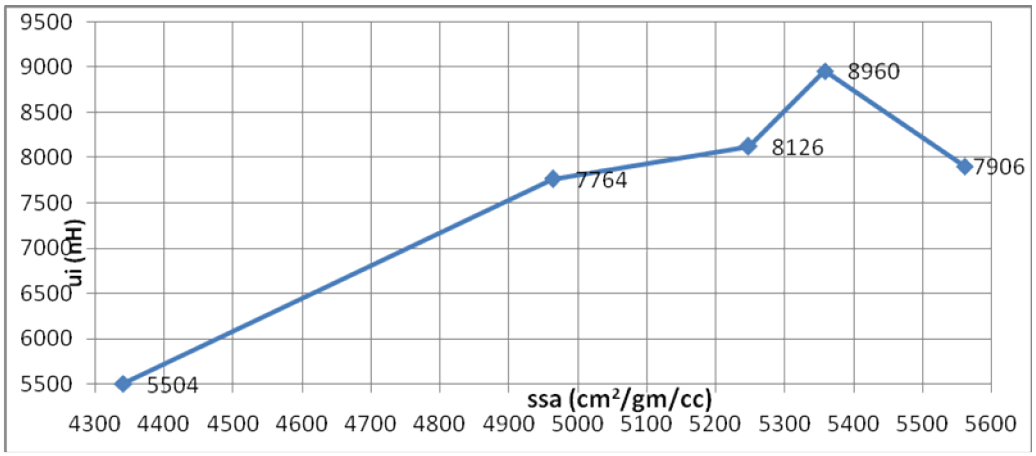

Figure 4.13 the variation of initial permeability at 10 KHz with specific surface area

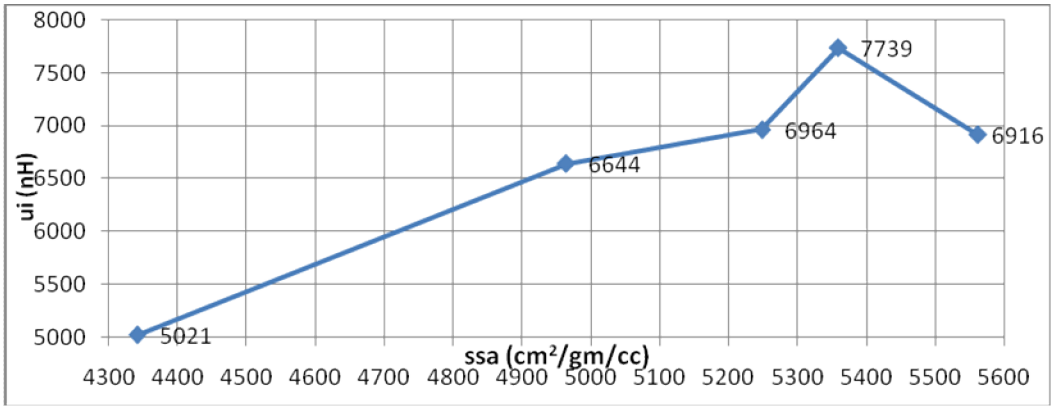

Figure 4.14 the variation of initial permeability at 100 KHz with specific surface area

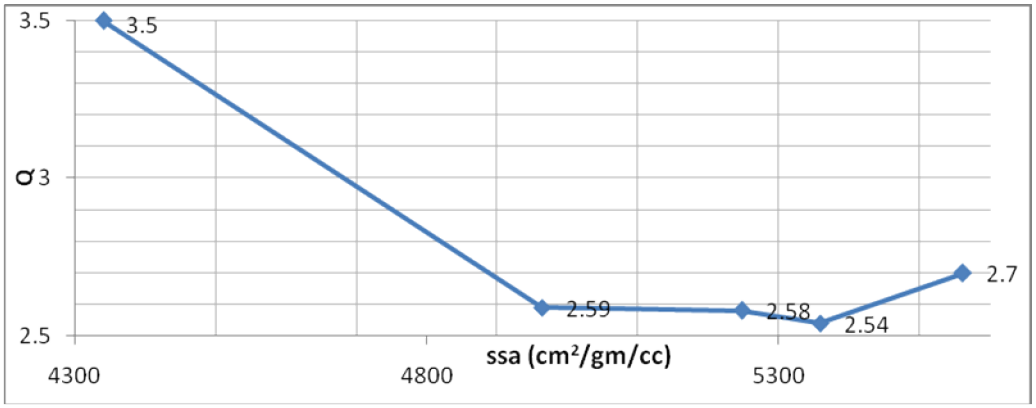

Figure 4.15 variation of quality factor (Q) with specific surface area

For low power loss materials, SSA affects electrical and magnetic property as at 5159 cm^2/gm SSA exhibits low power loss (69kw/m^3) and low resistance, while at 5468 cm^2/gm power loss increases (74kw/m^3) and resistance also increase.

For high permeability (μ_i) material, at 10 KHz and SSA 5359 cm^2/gm initial permeability exhibits higher (8960nH) and while at 5562cm^2/gm permeability decreases (7906nH). At 100 kHz and SSA 5359 cm^2/gm initial permeability exhibits higher (7739nH), while at 5562cm^2/gm initial permeability decrease (6917nH). The Quality factor is also affected at that point which is showing in figure 4.15.

4.3Ferrite phase formation (XRD)

The X-ray diffraction pattern of the dry mixed, pre-sintered and sintered crushed core powders are shown in figure-4.16, 4.17 and 4.18. These patterns reveal the sequential phase formation of Manganese-Zinc mixed ferrite from dry mixing to final sintering. All the peaks in the XRD pattern of sintered crush powder of the synthesized ferrite core are identified and indexed to (Zn Mn Fe) $(Fe\ Mn)_2O_4$. These patterns reveal the phase formation of Manganese-Zinc mixed ferrite.

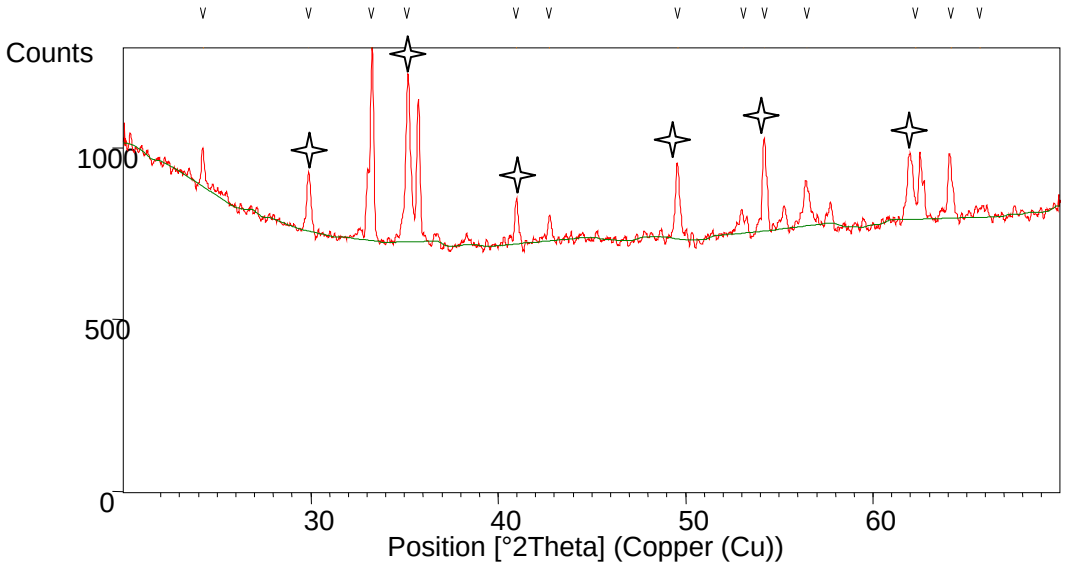

Figure 4.16 XRD pattern of sample-A Mn-Zn ferrite

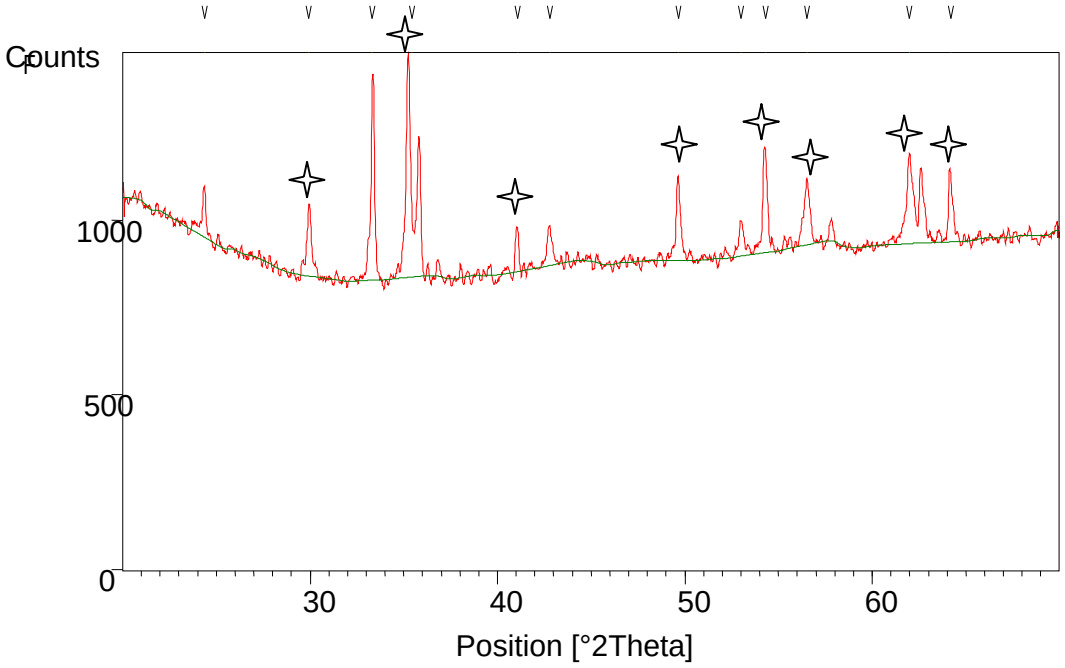

Figure 4.17 XRD pattern of sample-B Mn-Zn ferrite

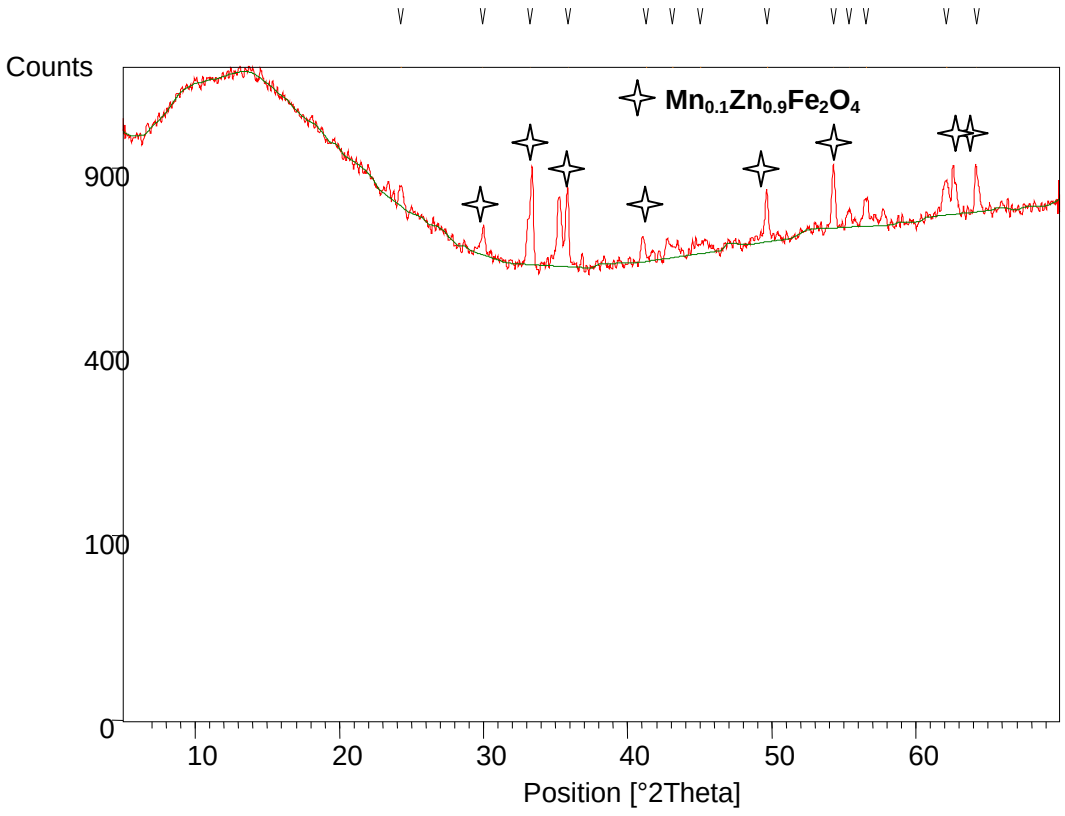

Figure 4.18 XRD patterns of sample-C Mn-Zn ferrite

The XRD pattern was indexed using JCPDS and Card number -742398. Single phase of $Mn_{0.1}$ $Zn_{0.9}Fe_2O_4$ has formed. The crystalline phase was same in all these samples indicating that concentration of binder has no effect on the nature of phase formed; however the crystalline peaks in case of sample-C had the least intensity as compared to other two samples. Due to less concentration of ferrite material effective scattering factor decreases and hence corresponding intensity of X-Ray diffraction from different plane decreases.[38]

4.4 **Thermo-gravimetric Analysis**

Thermo gravimetric plots obtained for the ready to press ferrite powder are shown in figure. Figure shows the binder burn out behaviour of the ferrite sample, binder burn out starts at about 150^0C and drastic loss in mass is observed up to 300^0C, complete binder burn out seems to occur at 400^oC. After the initial heating period in which the binder is burned off, the first chemical change occurs in the formation of zinc ferrite starting at 600^0C and continuing to about 800^0C. During this time Mn assumes its equilibrium form of Mn_2O_3. Shortly after 800^oC, Mn-Zn ferrite formation starts slowly with the dissolution of Mn into the Zinc ferrite. Due to higher heating rate, not much information can be extracted from figure. However, a continuous weight loss in the initial stage is observed.

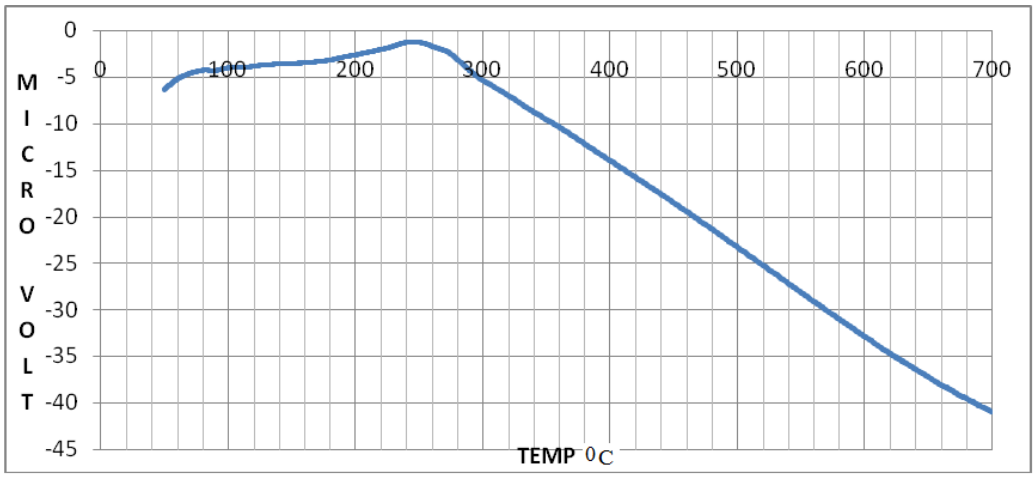

Figure 4.19 DTA measurements of a Mn-Zn ferrite powder at the heating rate of 10^0C/minute of sample-A

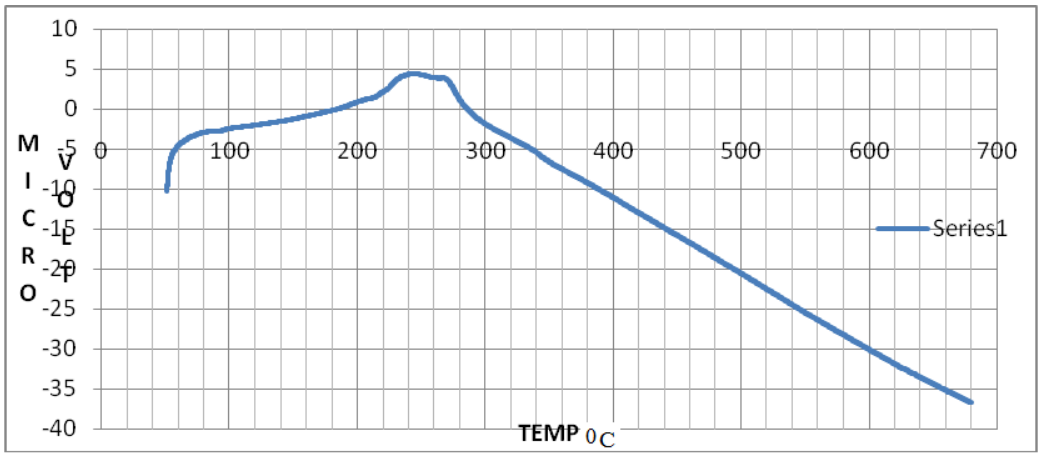

Figure 4.20 DTA measurements of a Mn-Zn ferrite powder at the heating rate of 10^0C/minute of sample-B

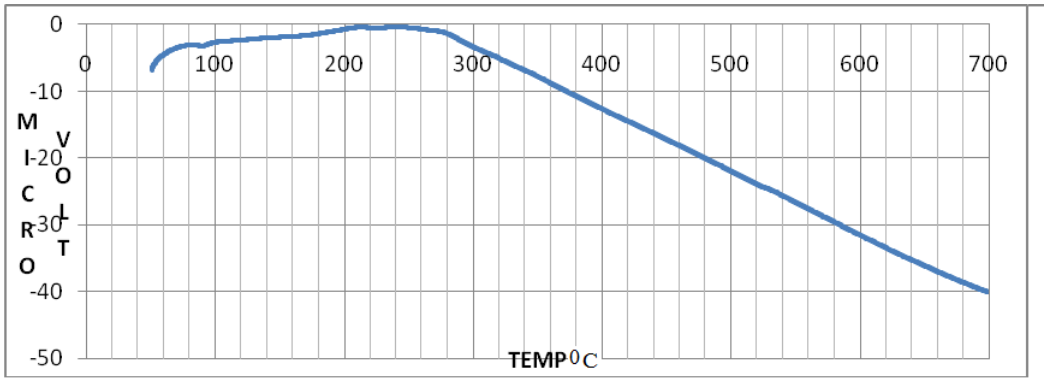

Figure 4.21 DTA measurements of a Mn-Zn ferrite powder at the heating rate of 10^0C/minute of sample-C

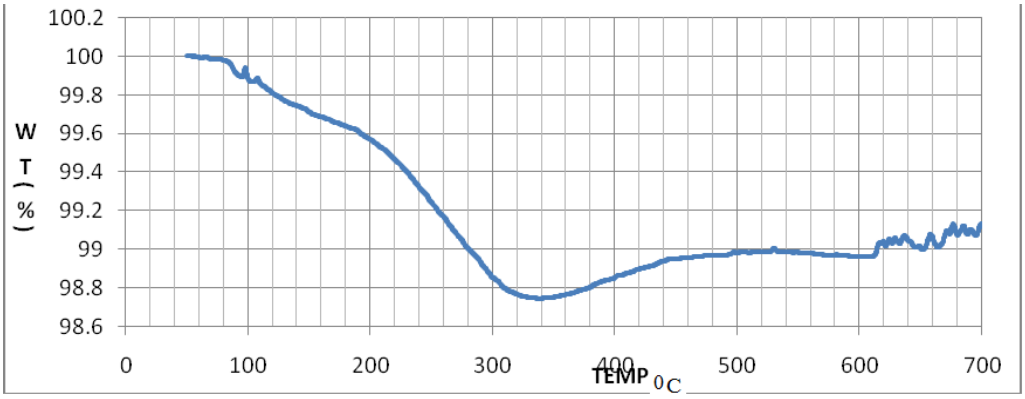

Figure 4.22 TGA measurements of a Mn-Zn ferrite powder at the heating rate of 10^oC/minute of sample-A

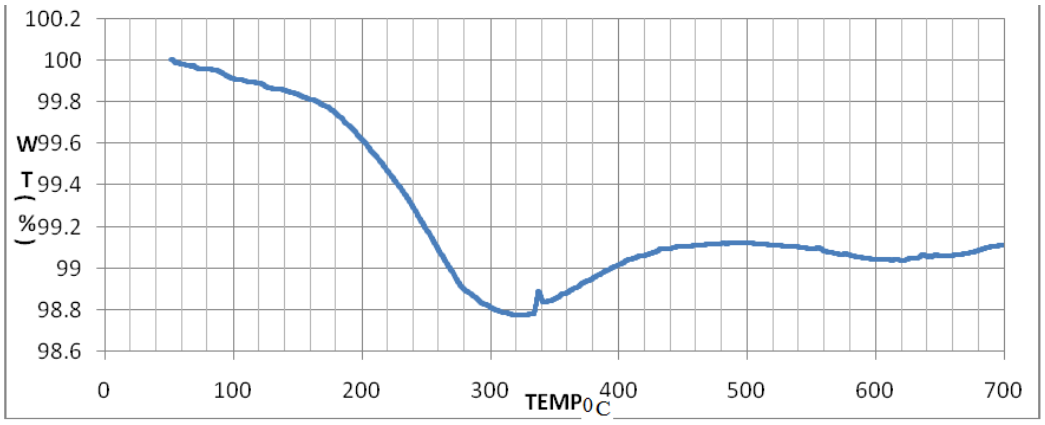

Figure 4.23 TGA measurements of a Mn-Zn ferrite powder at the heating rate of 10^0C/minute of sample-B.

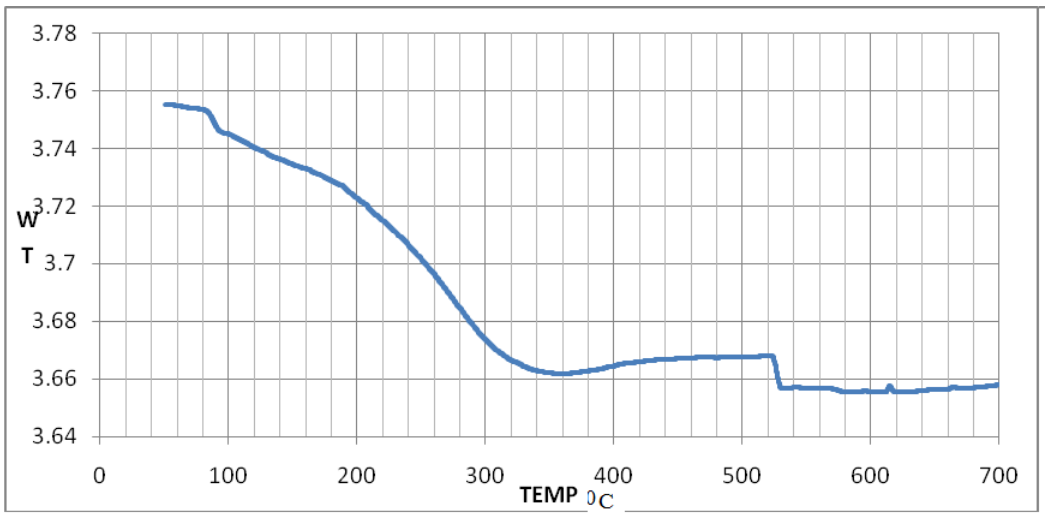

Figure 4.24 TGA measurements of a Mn-Zn ferrite powder at the heating rate of 10^oC/minute sample-C.

DTA curve provides data on the transformation that have occurred, such as glass transition, crystallization, melting and sublimation. The area under a DTA peak denotes the enthalpy change which is not affected by heat capacity of the sample. DTA curve can be used for indentification purpose, determination of phase diagram, heat change measurement and decomposition in various atmospheres. The exothermic reaction is caused by the oxidation of PVA to CO_2 and H_2O. Oxygen for this reaction is delivered either the oxygen of surrounding air atmosphere or the reduction of metal oxide in ferrite. Sample-C evaporation shifted between 50-100^0C due to moisture and

zinc stearate. TGA curve shows weight loss started with decomposition of MnO_2 to Mn_2O_3 at 525^0C for low binder [39]

$$2\ MnO_2 \longrightarrow Mn_2O_3 + O$$

Oxygen pick up take place at 300^0C and reach at 700^0C or more. So weight increase

$$2\ MnO_2 \longleftarrow Mn_2O_3 + O$$

$$Mn_2O_3 + 2Fe_2O_3 \rightleftharpoons 2MnFe_2O_4 + O$$

In sample-A sharp drop of weight loss at 150^0C and fast drop at 160^0C to 320^0C and binder burnout at 500^0C -650^0C.

4.5 SEM Micrograph of cracked Sample at different magnification

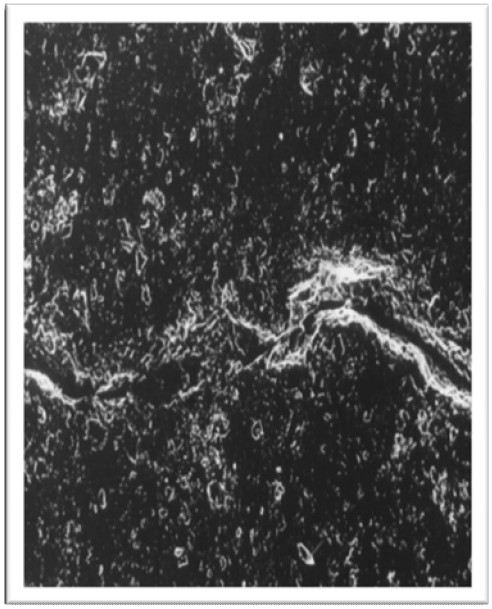

Figure4.25 SEM micrograph of cracked sample at 250X of Mn-Zn Ferrite

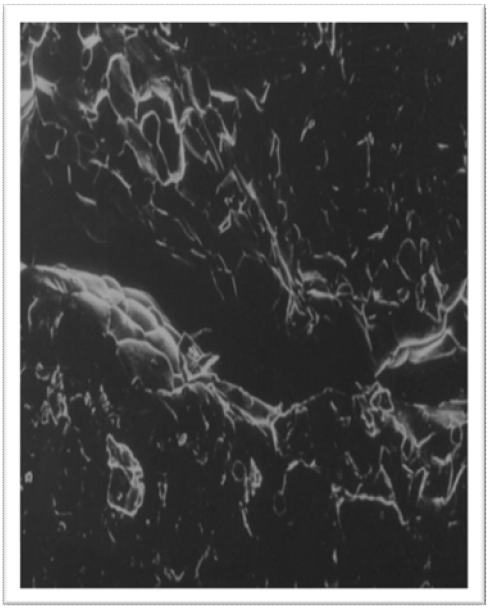

Figure4.26 SEM micrograph of cracked sample at 750X of Mn-Zn ferrite

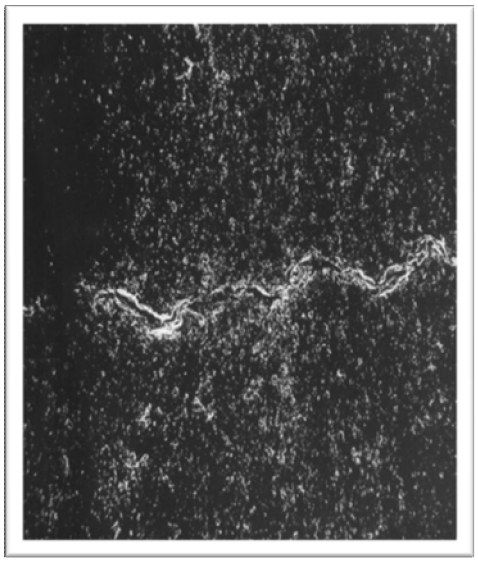

Figure4.27 SEM micrograph of cracked sample at 50X of Mn-Zn ferrites

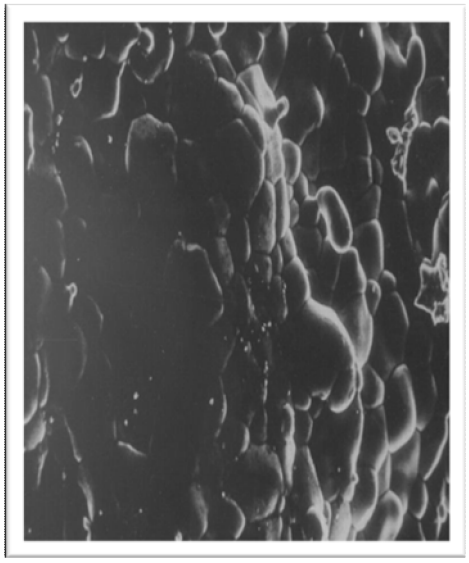

Figure4.28SEM micrograph of rough surface of cracked sample at 750X of Mn-Zn ferrite

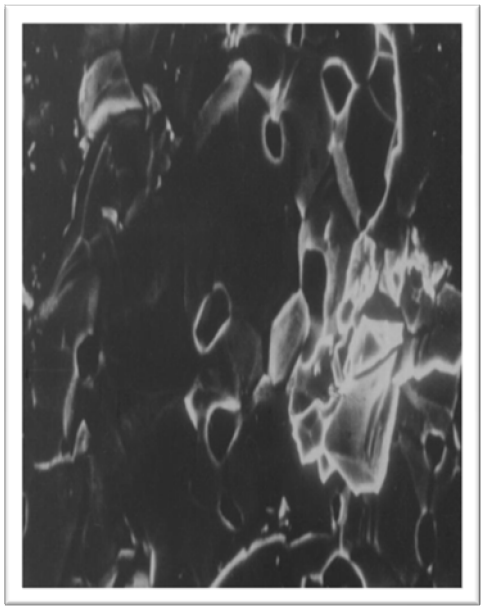

Figure 4.29 SEM micrograph of Mn-Zn ferrite at 1800X

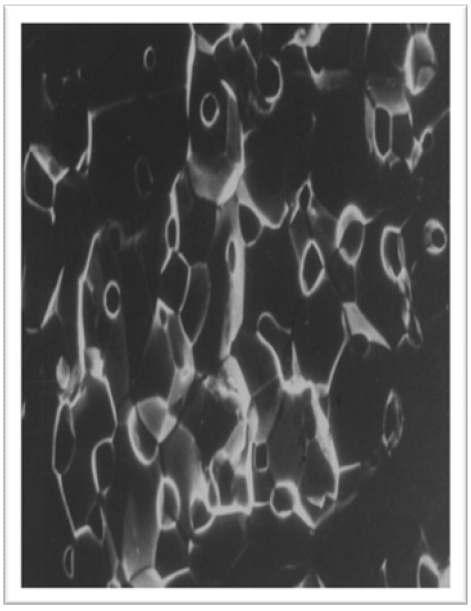

Figure 4.30 SEM micrograph of properly sintered surface at 1500X

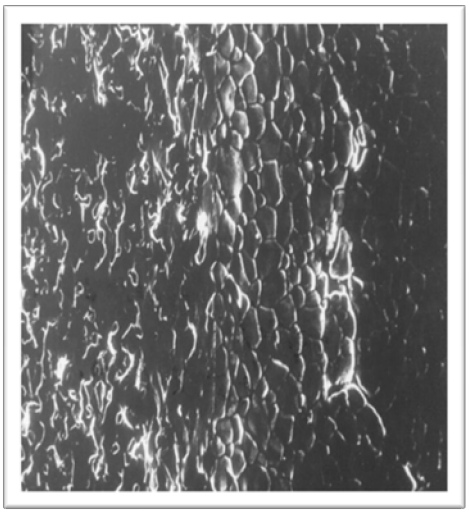

Figure 4.31 SEM micrograph of compression at 400X

Figure 4.32 SEM micrograph of Outer surface at 750 X

Figure 4.25, 4.26, 4.27 shows crack due to fast evaporation of PVA in debindering zone. It occurs in the temperature range from 25^0C to 600^0C where an exothermic reaction of binder burning occurs.[40] Figure 4.29 and 4.30 shows pores of sintered core of Mn-Zn ferrites. Figure 4.32 shows the micrograph of outer surface of the sintered core.

4.6. Microstructural Characterization

Microstructures of some selected etched samples at different magnifications are given in the figure. **Microstructure of low power loss material** (Sample 1, 2, 4, 6, 8)

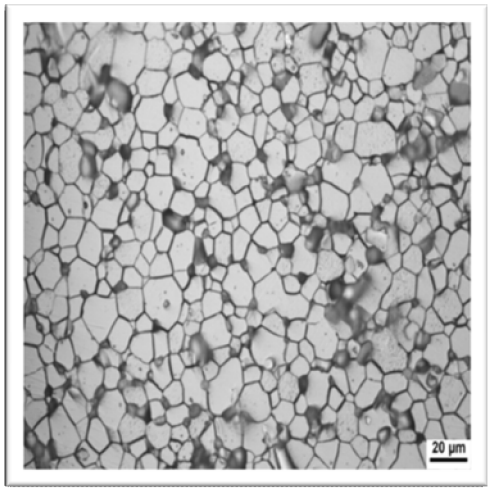

Figure 4.33 Optical Micrograph of Sample 1 at 500X, Inductance Factor=1850

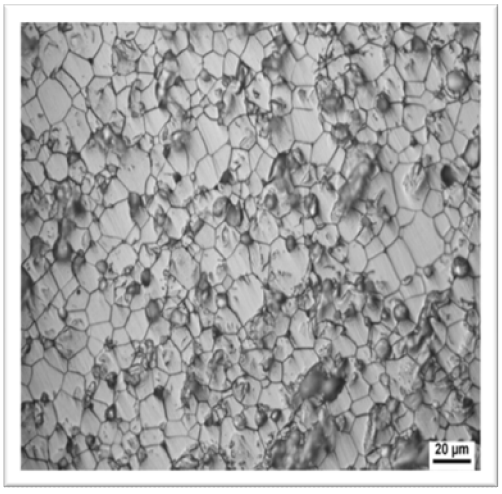

Figure 4.34 Optical Micrograph of Sample 2 at 500X, Inductance Factor=1979

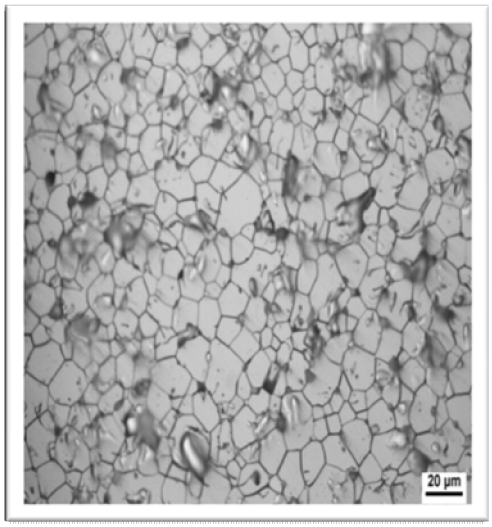

Figure 4.35 Optical Micrograph of Sample 4 at 500 X, Inductance Factor=1990

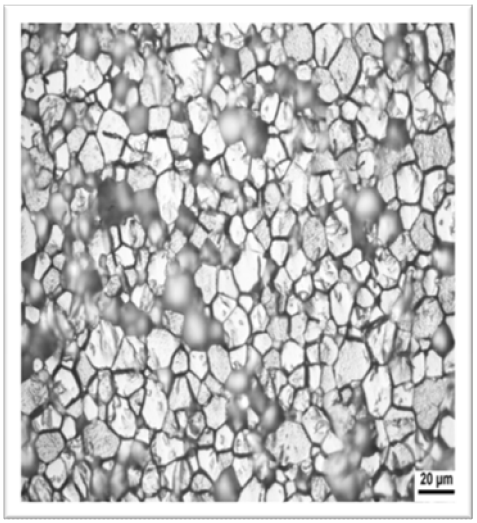

Figure 4.36 Optical Micrograph of Sample 6 at 500X, Inductance Factor=2160

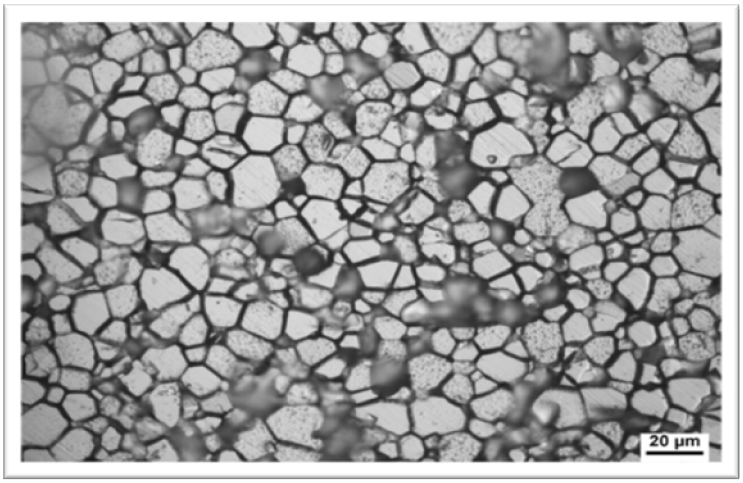

Figure 4.37 Optical micrograph of Sample 8 at 500X, Inductance Factor=2031

Microstructure of sample 6 which exhibits best inductance factor, low resistance and low power loss out of five samples studied is shown in figure 4.33-4.37 at a magnification of 500X. Similarly for sample 8 the structure obtained at 500X. Sample 8 exhibits more power loss than sample 6 due to CaO segregate around the grain boundaries to form a resistive layer and a distortion of the spinel lattice near the grain boundaries occurred due the incorporation of Ca atom in the spinel lattice and produced deletion effect on power loss property of Mn-Zn ferrites.[41]

Microstructure of high initial permeability Mn-Zn ferrite (sample 1, 2, 4, 6, 7)

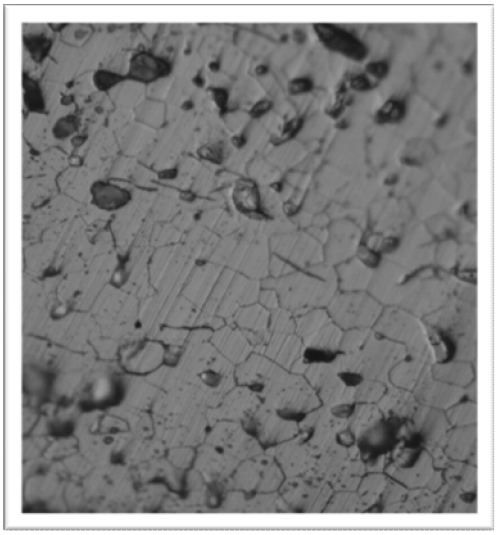

Figure 4.38 Optical micrograph of Sample 1 at 500X, permeability=5504

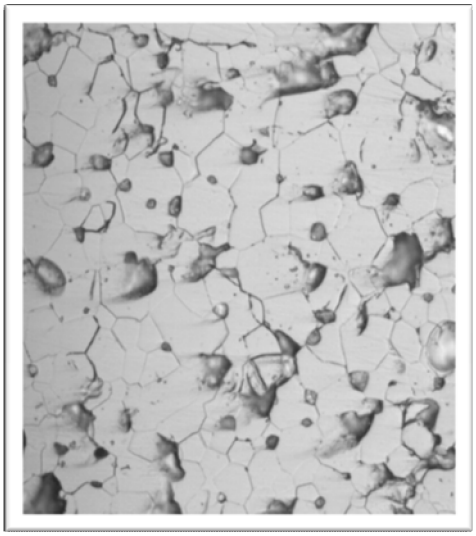

Figure 4.39 Optical Micrograph of at Sample 2 at 500X, permeability=7764

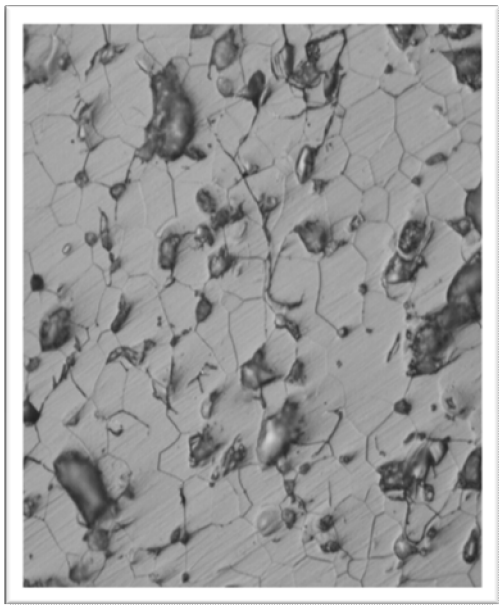

Figure 4.40 Optical Micrograph of Sample 4 at 500 X, Permeability=8126

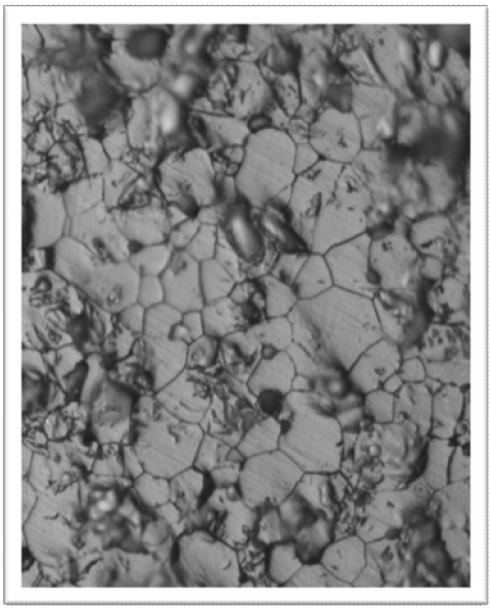

Figure 4.41 Optical Micrograph of Sample 6 at 500X, Permeability=8960

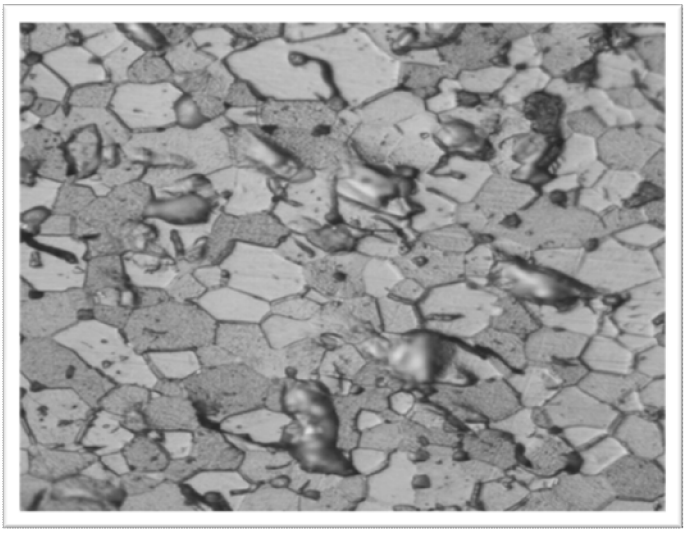

Figure 4.42 Optical Micrograph of sample 7 at 500X, permeability=7906

Microstructure of sample 6 which exhibits best permeability out of five samples studied is shown in figure 4.38-4.42 at a magnification of 500X. Similarly for sample 7 the structure obtained at 500X. We can see the difference in level of porosity in both samples. For the sample 7, porosity is higher as compared to sample 6. This is reason for decrease in permeability for decrease in permeability for sample 7 as compared to sample 6 as it has lesser grain boundary pinning effect. Similarly sample 1, 2, 4 which have lowest permeability out of prepared samples was studied microscopically and whose micrograph in shown in figure 4.35, 4.36, 4.37. Here we can see the highest porosity among all sample, resulting more grain boundary pinning and have lowest permeability value. [42]The reason of porosity is that, as Zn^{++} mole % is decreasing the mismatch between ionic radii of other constituents taking is increasing.

CHAPTER 5
CONCLUSION

The present work reports the study of Mn-Zn ferrite material of basic composition 51.96 mole% ferric oxide (99.8% Purity), 37.88 mole% manganese oxide (99% purity) and remaining 10.16 mole% zinc Oxide (99.5% purity), were mixed and blended homogenously through dry mixing in the pot mill for few hours and forming the chemical formula $Mn_{0.1}Zn_{0.9}Fe_2O_4$ with traces of some additives, suitable for power applications. X-ray diffraction pattern of the crushed powder of the sintered core reveals the formation of ferrite phase. The suitable combination of this ferrite composition with additives such as calcium oxide (500 ppm), bismuth oxide (150 ppm), niobium oxide (300 ppm) in desired quantity are added to the slurry in the ball mill and processed under strictly controlled sintering profile results in the prospective material for low power loss and high initial permeability (Table-4.4 and 4.5) application.

According to discussion in chapter-4 variation in specific surface area with milling time, the ball milling time can be reduce for maintaining required specific surface area. No more change in specific surface area in 3 to 5 Hrs because collision between ball and particle in ball milling will be low. The specific surface area are maintaining for achieving better electrical and magnetic property of the ferrites core. The bonding will be proper and spinal phase formed easily which gives better property. In ball milling the ratio of crushing of particle becomes constant so no more variation in that specific surface area.

For low power loss materials, specific surface area affects electrical and magnetic property as at 5159 cm^2/gm SSA exhibits low power loss ($69kw/m^3$) and low resistance while at 5468 cm^2/gm power loss increases ($74kw/m^3$) and resistance also increase. For high permeability (μ_i) material, at 10 KHz frequency and SSA 5359 cm^2/gm initial permeability exhibits higher (8960 nH) and while at $5562cm^2/gm$ permeability decreases (7906 nH). At 100 kHz frequency and SSA 5359 cm^2/gm initial permeability exhibits higher (7739 nH), while at $5562cm^2/gm$ initial permeability decrease (6917 nH).

According TGA Figure we should increase the cycle time in sintering because fast evaporation of PVA in debindering region in sintering process and abrupt weight reduction at 520-540^{0}C for high binder Mn-Zn ferrite. The SEM microstructure shows that cracks occur due to PVA fast evaporation of binder in debindring Zone.

The microstructural study shows high initial permeability material (sample 6) exhibit high permeability and low porosity at specific surface area (5359 cm^2/gm) and low power loss material exhibits low power loss at specific surface area (5169 cm^2/gm).

It is the most promising candidate for being applicable in regular switching power supplies, as well as in main transformers in DC-DC converters for electrical vehicles such as hybrid electrical vehicles. This material can be shaped to any core design and can be used in the Inverter transformers for LCD backlight, AC adapters and chargers of notebook type PC's.

It is used in computer, radio-communication and interference suppression, SMPS for wide-band transformers, power transformers and pulse transformers, TV applications, industrial and professional applications for wide-band transformers and high voltage transformer. Soft ferrite cores are used in a large band of applications, with different shapes and adapted materials.

CHAPTER 6
SCOPE OF THE FUTURE WORK

The modern devices exclusively need soft magnetic materials as its basic component. Soft ferrite material is extensively used in inductors, transformers, antenna rods, loading coils, deflection yokes, choke coils, recording heads, magnetic amplifiers, electromagnetic interference (EMI), power transformer, lighting and splitter applications, which forms a basic requirement in high technology areas. Mn-Zn ferrites adequately suit these demands and are considered to shape the future advanced technology. It is the need of hour to reduce the power loss at high frequency in order to meet the current demand of the high efficiency and miniaturization of the electronic devices. Mn-Zn ferrite material with these properties will certainly enhance fuel efficiency, electric-power saving. The variation of power loss and initial permeability with specific surface area of Mn-Zn Ferrite can use our market demand and products.

These extremely outstanding characteristics could be realized by

- Accurate estimation of the composition and specific surface area, taking into account magnetic anisotropy and grain boundary resistivity.
- The use of ultra pure and ultra fine raw materials.
- Proper and appropriate selection of particle size to meet the grain boundary resistivity requirements.
- Strict and precise control of oxygen partial pressure of the sintering atmosphere.

REFERENCE

[1]. R.F. Louh, T.G. Reynolds III and R.C. Buchanan, Ceramic Materials for Electronics, 3rd edition, edited by R.C. Buchanan, Marcel Dekker Inc. (2004).

[2]. Soft ferrite A user Guide's magnetic materials producers association , 8 south Michigan, suite 1000, Chicago, IL 60603

[3]. Chikazumi, S. 1964. Physics of Magnetism, New York: john Wiley & sons

[4]. R. Justin Joseyphus, A. Narayanasamy, K. Shinoda, B. Jeyadevan and K. Tohji, J. Phys.Chem. Solids .

[5]. B. Jeyadevan, C. N. Chinnasamy, K. Shinoda, K. Tohji and H. Oka, J. Appl. Phys. 93, 8450 (2003).

[6]. J. Smith and H. P. J. Wijn, in Ferrites, New York: John Wiley, 1959, p. 369.

[7]. C. Rath, S. Anand, R. P. Das, K. K. Sahu, S. D. Kulkarni, S. K. Date and N. C. Mishra, J. Appl. Phys. 91, 2211 (2002).

[8]. B. Jeyadevan, K. Tohji, K. Nakatsuka and A. Narayanasamy, J. Magn. Magn. Mater. 217, 99 (2000).

[9]. S. Son, R. Swaminathan and M. E. McHenry, J. Appl. Phys. 93, 7495 (2003).

[10]. K. Tkácová, V. Šepelák, N. Števulová, and V. V. Boldyrev, J. Solid State Chem. 123, 100 (1996).

[11]. K. T. Han, B. D. You, D. S. Kang, W. G. Kwon and S. H. Choi and Seung Wha Lee, J. Korean Phy. Soc. 28, 614 (1995).

[12]. S. W. Lee, S. I. Park, S. B. Kim, C. S. Kim and H. N. Ok, J. Korean Phys. Soc. 31, 504 (1997).

[13]. K. Ohta,; Kobayashi, N. Jpn. J. Appl. Phys. vol. 3, 1964, p. 576–580.

[14]. H. Tsunekawa, A. Nakata, T. Kamijo, K. Okutani, R. K. Mishra, and G. Thomas, IEEE Trans. Mag. MAG-15(6), 1855 (1979).

[15]. A. Žnidaršič, M. Limpel, M. Drofenik, "Effect of Dopants on the Magnetic Properties of Mn-Zn Ferrites for High Frequency Power Supplies", IEEE Trans. Mag. 31(1995)2, 950-953.

[16]. M. Drofenik, A. Žnidaršič and I. Zajc, "Highly Resistive Grain Boundaries in Doped Mn-Zn Ferrites for High Frequency Power Supplies", J. Appl. Phys. 82(1997)1, 333- 340.

[17]. Stoppels, D., Developments in soft magnetic power ferrites. J. Magn.Magn.

Mater. 1996, 160, 323–328.

[18]. T. Akashi, Trans. Japan. Inst. Metals 2, 171 (1961). 76

[19]. H. Tsunekawa, A. Nakata, T. Kamijo, K. Okutani, R. K. Mishra, and G. Thomas, IEEE Trans. Mag. MAG-15(6), 1855 (1979).

[20]. A. Znidarsic, M. Limpel, G. Drazic, and M. Drofenik, in ‘‘Ferrites:- Proceedings of The Sixth International Conference on Ferrites,Tokyo,’’ ICF6, p. 333, 1992.

[21]. Alex Goldman, Modern Ferrite technology

[22]. Drofenik , et al. 1985. Advances in Ceramics 16, 229

[23]. Roess, E. 1285. Advances in ceramics 15, 38.

[24]. Yoneda, N., 1980. Ceramic Bull. 59,549.

[25]. Globus, A., 1972 phys. Stat. solid. 52, 427.

[26] A. Handstein, K.H. Muller, R. Grossinger, H.R. Kirchmayr and R. Krewenka, Influence of particle size on the properties of polymer bonded NdFeB magnets

[27].Magnetics, IEEE Transactions on Publication Date: Jan. 2000 volume : 36, issue :1, part-2 on page (s) : 375-380.

[28]. Matsuo, Y.; Ono, K.; Hashimoto, T.; Nakao, F. Magnetics, IEEE Transactions on Volume 37, Issue 4, Jul 2001 Page(s):2369 – 2372 Digital Object Identifier 10.1109/20.951175

[29]. A. J. Pigram & R. Freer, the Effect of Binder Additions on the Green and Sintered Properties of Mn-Zn Ferrite Ceramics, Ceramics International 21 (1995) 33-41.

[30]. Stanley J. Lukasiewicz, Spray-Drying Ceramic Powders, J Am. Ceram. SOC, 72 141 617 24 (1989).

[31]. Effect of External Lubricant on Mechanical Properties of Dry-Pressed Green Bodies, Maruti Uppalapati and David J. Green, J. Am. Ceram. Soc., 88 [6] 1397 1402 (2005).

[32]. Jillavenkatesa A, Dapkunas S J, Lin-Sien Lum, Particle Size Characterization, NIST Special Publication 960-1, 2001

[33] Sivakugan N, Soil Classification, James Cook University Geoengineering lecture handout, 2000 .

[34]. James P M Syvitski (editor) (2007). Principles, Methods and Application of Particle Size Analysis. Cambridge University Press.

[35] http://goldbook.c60.kiev.ua/S05806.pdf IUPAC Compendium of Chemical Terminology 2nd Edition (1997).

[36] http://web.archive.org/web/20060905224652/http://www.soils.wisc.edu/ss322/lctures/lec+8-11.pdf

[37].Ceramic processing and sintering by M.N. Rahaman,chapter-2 syenthesis of powder, page number 46.

[38]. X- Ray diffraction by B.D.Koulty.

[39].Th.G.W.Stijntjes, J.J. Roelofsana,L.H. Boonstra and W.M. Dawson in ‘‘Ferrites Proceedings of The Sixth International Conference on Ferrites,Tokyo,’’ ICF6, p. 45, 1992.

[40]. A.J. Pigram and R.Freer in ceramic international 21 (1995) 33-41.

[41].Ammad H. Qureshi Journal of Crystal Growth October 2005

[42]. Prinya Sainamthip and V.R.W. Amarakoon, J. Am. Ceram. Soc. 71(8) 644-48 1988